REVIEW

Applications of coulometric titration for studies of oxygen non-stoichiometry in oxides

**Mikhail V. Patrakeev · Ilia A. Leonidov ·
Victor L. Kozhevnikov**

Abstract This article gives a brief overview of the modern methods for in situ studying of oxygen non-stoichiometry in oxides. The emphasis is on the techniques that are based on the use of transport properties of solid electrolytes with unipolar oxygen ion conductivity, as well as on the experimental implementation of coulometric titration. The possible sources of experimental errors are considered, and methods are discussed of their accounting and minimization. Several examples are given of the using of the data on non-stoichiometry for the determination of thermodynamic properties and defect structure in oxides.

Keywords Oxides · Oxygen non-stoichiometry ·
Thermodynamics · Solid electrolytes

Introduction

Measurement of high-temperature thermodynamic properties is a conventional and highly informative approach to the examination of the defect structure of oxides. The interpretation of data is based on the possibility of description of defects in terms of chemical potentials. Generally, an oxide crystal admits both ionic and electronic defects. The ratio between their concentrations and consequently between respective contributions to electron and mass transport depends on the character of impurities, statistical and energy parameters, temperature T, and oxygen activity p_{O_2} in the gaseous phase. In the simplest cases, the concentration of defects is proportional to $p_{O_2}^{\pm 1/n} \exp(-\Delta H/RT)$, where the

baric pre-exponent depends on the nature of equilibrium defects, while the exponent parameter is the defect formation enthalpy [1]. If defects are formed in the oxygen sub-lattice, this parameter is partial formation enthalpy of the corresponding oxygen defect, and it can be determined directly from the relationship between the equilibrium oxygen content in oxide and parameters of the surrounding gaseous phase. Since deviations of oxygen content in oxides from the stoichiometric composition are usually designated as δ, such dependences are called $p_{O_2} - T - \delta$ diagrams. Formation of oxygen defects in the crystal lattice often leads to a variation in the charge state of cations. Analysis of $p_{O_2} - T - \delta$ diagrams is helpful in order to find corresponding defect equilibrium reactions, to calculate equilibrium constants and concentrations of cationic defects, and to study their association with oxygen defects. Different point-defect schemes are outlined for the description of oxygen non-stoichiometry data in [2]. In oxides with wide oxygen homogeneity regions, the concentration of ionic and electronic defects is often comparable with the concentration of regular sites. In such cases, the parameters and the general configuration of equilibrium $p_{O_2} - T - \delta$ diagrams are closely connected with the energy characteristics of the electronic subsystem [3, 4], and point-defects models rarely result in a satisfactory understanding of the defect architecture in these oxides.

In this work, different experimental approaches to plotting $p_{O_2} - T - \delta$ diagrams are briefly considered. However, the main concern is with the electrochemical methods, which are based on transport properties of solid oxygen electrolytes and make it possible to vary, with a high accuracy, the amount of oxygen in a given volume and to measure its activity. Such methods are usually termed coulometric titration. Possible ways of implementation of these methods are considered. Factors that influence the

M. V. Patrakeev (✉) · I. A. Leonidov · V. L. Kozhevnikov
Institute of Solid State Chemistry, Ural Branch of RAS,
91 Pervomaiskaya Str.,
Yekaterinburg, Russia
e-mail: patrakeev@ihim.uran.ru

precision and reproducibility of measurements are analyzed. Certainly, it is impossible to give an exhaustive description of all studies related to this subject within a single publication. Therefore, we made an attempt to trace only the basic aspects in the development of coulometric titration methods with the use of some works as an example. We also give examples showing how the $p_{O_2} - T - \delta$ diagrams can be applied for obtaining information about properties of non-stoichiometric oxides.

General techniques for in situ measurements of oxygen stoichiometry

Variations in the equilibrium state of oxide

$$MO_n \rightleftarrows MO_{n-\delta} + \frac{\delta}{2}O_2 \qquad (1)$$

with changes in temperature and/or oxygen pressure can be observed from variations in a sample's mass, gaseous phase composition, or gaseous phase pressure. An oxide is in equilibrium with the gaseous phase if the chemical potentials of oxygen $\mu_O^{MO_{n-\delta}}$ and μ_{O_2} in the oxide and in gaseous phase, respectively, are equal:

$$\mu_O^{MO_{n-\delta}} = \frac{1}{2}\mu_{O_2} \qquad (2)$$

Modern electrochemical methods permit highly precise measurements of the chemical potential of oxygen in the gaseous phase. They constitute the basis of the technique for examination of equilibrium (1), namely, the coulometric titration method. One more method should be mentioned also—neutron powder diffractions that are based on neutron scattering in solids. Recent advances facilitate the wider use of this technique for in situ determination of oxygen content in oxides.

Regardless of the experimental approach, measurements of oxygen non-stoichiometry as a function of temperature and oxygen activity take much time, which is determined by oxygen diffusion rate in oxides and by the rate of exchange reactions on the surface. To accelerate equilibration with the gaseous phase, samples are usually used in the form of powders. To obtain a detailed $p_{O_2} - T - \delta$ diagram, an experiment may last as long as several hundred hours. Undoubtedly, with such a considerable duration, particular attention should be paid to the computerization of measurements. Note that the measured parameter (e.g., mass or oxygen pressure) is recorded tens of times during equilibration. In this process, a relaxation curve is formed, which is a characteristic of exchange kinetics between a sample and gaseous-phase oxygen and oxygen diffusion rate in the sample. Analysis of such relaxation dependences allows estimation of the corresponding kinetic coefficients [5–9].

Thermo-gravimetric measurements

The gravimetric method for monitoring the equilibrium (1) is the simplest and therefore the most frequently used technique. For its realization, different commercial devices for thermo-gravimetric analysis (TGA) are widely applied [5–19]. Thermo-gravimetric measurements permit the estimation of oxygen non-stoichiometry as

$$\delta = \delta_{ref} + \frac{M_s}{m_s M_O}\Delta m \qquad (3)$$

where M_s and m_s are the molar mass and the sample mass of the stoichiometric oxide, respectively, M_O is the atomic mass of oxygen, and Δm is the variation in the sample mass under equilibrium conditions relative to the state with the known oxygen content δ_{ref}. According to expression (3), measurement accuracy is determined by the sample mass and by balance resolution. Usually, m_s is ~0.1 g. Sometimes, in order to improve the accuracy, especially when studying oxides with relatively small oxygen homogeneity regions, samples of 1 g [12, 16, 17] and even 3–4 g [19] are used. The absolute error of the method is typically $\Delta\delta = \pm 0.001$ [10, 15]. The method is convenient because it has practically no temperature limitations since the control mechanism of balance is at room temperature. Generally, variations in the sample mass may occur not only as a result of oxygen exchange but also as a consequence of water discharge, release of volatile oxides, or evaporation. The nature of the respective process cannot be established directly by means of a thermoanalyzer. Therefore, the measuring device is completed with equipment for evolved gas analysis if necessary. For example, the mass spectrometer is used in [19]. Although the programmable temperature mode is an integral function of TGA devices that facilitates measurements in isobaric conditions, oxygen non-stoichiometry measurements are more often performed in the isothermal runs [10–14, 16, 17]. To obtain experimental data in a wide range of partial pressures of oxygen, attested gas mixtures O_2–Ar, CO–CO_2, and H_2–H_2O–Ar, which have required ratios of components, are usually used. Stable gas mixture flow in the thermoanalyzer operation zone is provided by mass flow meters [10, 14]. The flow rate is determined by the analyzer design features, the sample characteristics, and the gas composition and may vary from 30 [19] to 150 ml/min [14, 16, 17]. For additional assurance that equilibrium between the sample and the gas phase is attained, the activity of oxygen in the gas mixture at the analyzer outlet is monitored with yttria-stabilized zirconia (YSZ) oxygen sensors [8, 13–17]. The most serious problem in the application of the gravimetric method occurs at low oxygen pressure $\left(p_{O_2} < 10^{-4} \text{ atm}\right)$. In these conditions, gas exchange may lead to a considerable local deviation in partial pressure of oxygen in the vicinity of

the sample from the assigned value in the gas mixture. To reduce the corresponding error, the activity of oxygen must be monitored immediately near the sample. Though this problem is connected with procedure difficulties, the technique of gravimetric experiments is constantly progressing, which allows improving the quality of measurement results. For example, in [10, 11], the oxygen partial pressure was in situ measured by a YSZ sensor in close vicinity to the sample. Good experimental arrangement was demonstrated in [20], where oxygen non-stoichiometry of chromites $La_{1-x}Ca_xCrO_{3-\delta}$ was studied. Samples for measurements were prepared as rods with a relative density 50–65%. Thermogravimetric measurements were performed by using an electronic microbalance connected to a reaction tube and a gas flow system. The schematic view of the measuring system is shown in Fig. 1. A sample rod was suspended from the electric microbalance. The temperature around the sample was controlled within 1 K from that desired. The weight change due to oxygen non-stoichiometry of $La_{1-x}Ca_xCrO_{3-\delta}$ was measured in an oxygen-controlled atmosphere by the use of O_2–Ar, CO–CO_2, and H_2–H_2O–Ar gas mixtures at 1073–1373 K. Three YSZ oxygen sensors were equipped for monitoring p_{O_2}. The gas mixture was allowed to flow through a bypass line to a zirconia oxygen sensor to confirm the prepared p_{O_2}. After confirmation of stable p_{O_2}, the gas mixture was passed through the reaction tube to the sample. A zirconia sensor was also placed in the reaction tube to monitor p_{O_2} near the sample. The sample reached the equilibrium with the gaseous phase, when both the weight of the sample and p_{O_2} in the reaction tube became stable. For buoyancy corrections in different gas compositions, the apparent weight change of a dense alumina was measured in different gas mixtures between 1073 and

1373 K. Alumina is considered to have no oxygen non-stoichiometry here. After the buoyancy compensation, the uncertainty of the weight measurements was ±60 μg. The accuracy of δ of $La_{1-x}Ca_xCrO_{3-\delta}(x = 0.1, 0.2)$ and that in $La_{1-x}Ca_xCrO_{3-\delta}(x = 0.3)$ was considered to be within 0.0005 and 0.0009, respectively. The difference originated from the weight of each sample [20].

Thus, the thermo-gravimetric method in its modern implementation ensures very accurate measurements of oxygen non-stoichiometry in oxides in a wide range of temperature and oxygen partial pressure. The application of commercial equipment for measurements makes this method particularly popular.

Volumetric measurements

Research into high-temperature superconductivity raised considerable interest in studying oxygen non-stoichiometry in oxides since the properties of oxide superconductors depend strongly on the content and distribution of oxygen in the crystal lattice [21–26]. One of the most detailed $p_{O_2} - T - \delta$ diagrams for the famous compound $YBa_2Cu_3O_{6+\delta}$ was obtained in [27]. There, oxygen non-stoichiometry was studied with the use of a computer-controlled volumetric system shown in Fig. 2. The method was based on monitoring the oxygen pressure in the gas phase, which was in equilibrium with the sample. The high-vacuum apparatus (base pressure ~10^{-7} mbar) consisted of a gas chamber and a sample chamber, both of known volumes, a pressure transducer, a gas handling system, and a pumping unit. The sample chamber was a quartz tube with a small inner Pt crucible containing powdered $YBa_2Cu_3O_{6+\delta}$ (grain size ~20–70 μm). The sample side of the chamber was

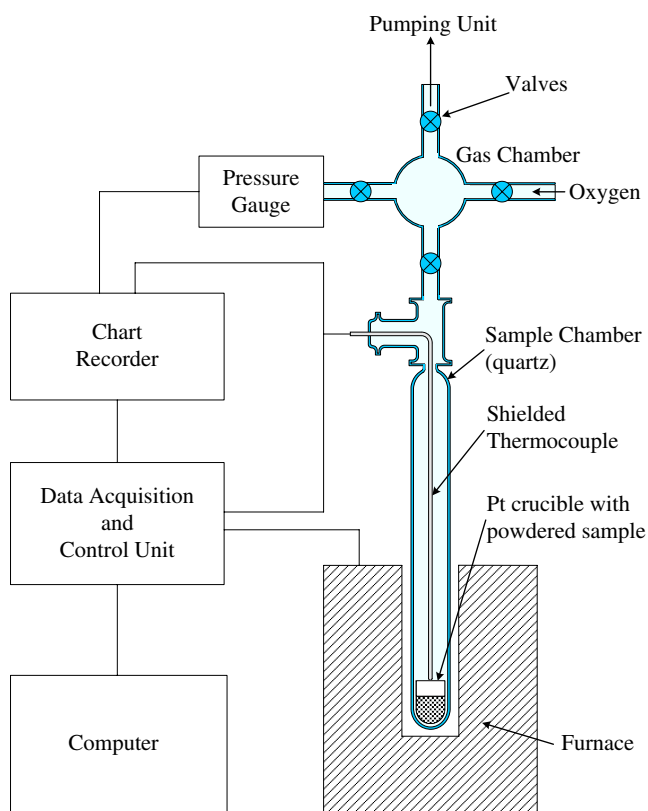Fig. 1 A sketch of the system for thermogravimetric measurements [20]
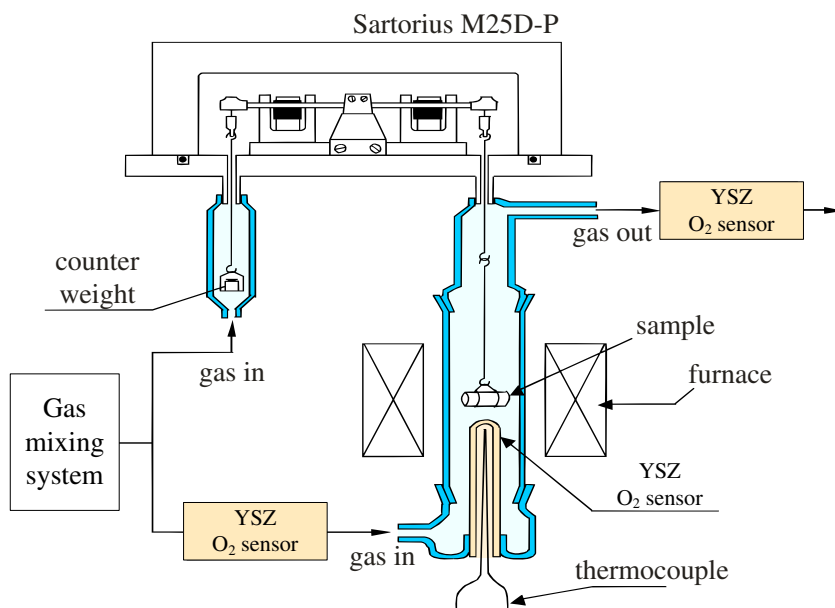
Fig. 2 A schematic representation of the system for measurements of the pressure–composition isotherms by volumometric technique [27]

placed in the heating zone of a tubular furnace. The sample temperature was measured by a shielded thermocouple (NiCr–Ni) attached to the Pt container. Before starting an absorption cycle, the powder was first subjected to a desorption procedure to achieve an initial oxygen content of $\delta \approx 0$ as a reference state. This was accomplished by degassing the powder in vacuum, applying a linear heating rate of 2 °C/min up to 750 °C, and then holding at this temperature for 1 h. This process led to the oxygen content $\delta = 0$, verified by the fact that, in a subsequent recharging experiment (slow cooling to room temperature at 0.75 °C/min under an oxygen pressure of about 1300 mbar), the maximum amount of absorbed oxygen was 1 ± 0.013 mol of oxygen atoms per mole of $YBa_2Cu_3O_{6+\delta}$. Then, the oxygen content at a given pressure and temperature could be evaluated by ideal gas law calculations, as sample mass, sample chamber and gas chamber volumes, pressure difference due to oxygen uptake, and effective gas temperature were known. In applying the effective temperature correction, the non-uniform temperature distribution within the connected gas and sample chambers was taken into consideration. The effective gas temperature was obtained experimentally by carrying out various runs similar to the absorption measurements without a sample inside the sample chamber. Oxygen non-stoichiometry in

$YBa_2Cu_3O_{6+\delta}$ was studied in the isothermal mode in the interval 400–750 °C at oxygen pressure varying between 1 and 1500 mbar. Uncertainties in the composition, δ, were estimated to be of the order of ±3–4% for compositions belonging to the high pressure branches of the isotherms (around 1000 mbar) and ±1–2% for compositions belonging to the low pressure branches (around 10 mbar). These uncertainties were due to errors in the pressure and temperature readings during the absorption cycles and errors in volume and effective gas temperature calibrations [27]. The large body of experimental points, Fig. 3, made it possible to reconstruct in detail the behavior of oxygen partial thermodynamic functions depending on oxygen content in the cuprate, in particular, in the region of orthorhombic to tetragonal structure transition. The data obtained were used in [28] to describe defect formation and ordering processes. Although the volumetric method is used in oxygen non-stoichiometry studies rather infrequently, the authors succeeded in its advantageous realization. In particular, the barometric sensor provided oxygen pressure measurements at comparatively low temperatures, whereas uncontrolled oxygen leaks in the system were eliminated owing to the quartz operation chamber. As a particular advantage, the volumetric method applies no stringent restrictions on the sample mass. Besides, the carefully made gas distribution system ensured high oxygen pressure resolution. The drawback of the method is non-isothermal operation gas space, which hampers the determination of the quantity of oxygen in a known volume at a known pressure. The authors of [27] solve this problem by a preliminary calibration and determination of "effective
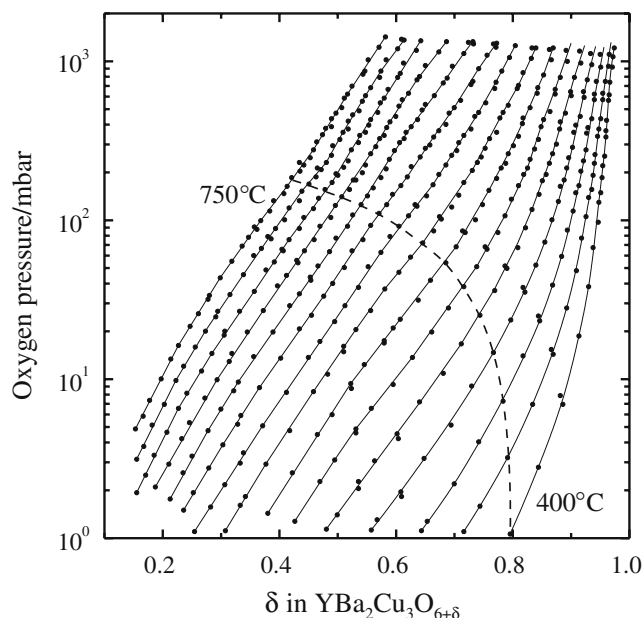

Fig. 3 Pressure–composition isotherms for oxygen in $YBa_2Cu_3O_{6+\delta}$. The temperature step between isotherms is 25 °C [27]

temperature". However, such an experimental approach results in decrease of measurement precision. An essential limitation of the method is that measurements must be carried out in the atmosphere containing no other gases but oxygen. Therefore, the low-pressure region $p_{O_2} < 10^{-5}$ atm, where oxygen activity is determined by the ratio of components in special gas mixtures, is beyond the applicability of the volumetric method.

Neutron diffraction

A promising technique for oxygen non-stoichiometry studies is in situ neutron powder diffraction (NPD). Neutron scattering lengths of oxygen and, e.g., of iron and strontium have comparable values, and the measurements are almost equally sensitive to all three elements [29]. In contrast to X-ray diffraction, this method permits determining both the coordinates and the population of oxygen sites. The extensive use of the method is limited since such studies must be performed within special facilities equipped with a high-power neutron source. Taking into account the considerable time necessary for deriving a large body of $p_{O_2} - T - \delta$ data, it is easy to see that such experiments may be quite costly. The certain benefit of the method is that the diffraction spectrum contains information about the absolute content of oxygen. On the other hand, interpretation of diffraction results is a complicated multifactor problem, and its solution does not always lead to high accuracy in oxygen content determination. A good example is research [29], in which the high-temperature modification of strontium ferrite, $Sr_2Fe_2O_5$, was examined. It was observed that 20 oxygen ions are randomly distributed over 24 available sites. The refinement of the oxygen occupancy factor resulted in 19.66 oxygen atoms per unit cell, which is suggestive of a considerable amount (8.5%) of iron in 2+ oxidation state. On the other hand, precise analytical measurements do not confirm even a trace concentration of Fe^{2+}. This disagreement is indicative of the uncertainty no less than 0.085 per formula unit of $Sr_2Fe_2O_5$ in oxygen content calculated from NPD results [29]. In [30], in situ neutron diffraction was employed to study oxygen non-stoichiometry in $SrCo_{0.8}Fe_{0.2}O_{3-\delta}$ at 873–1173 K and oxygen partial pressure $5\cdot10^{-4}$–1 atm. Diffraction patterns were collected during slow heating ramps, 1.33 K/min, between 873 and 1273 K, while continually flushing the sample with the calibrated gas mixture and monitoring the outlet p_{O_2}. The measurement time for each diffraction pattern depended on the intensity of the incoming beam and resulted in a temperature spread between 5 and 10 K for each measurement. The measurements were made in descending p_{O_2} starting at 1 atm. Before measurements at $p_{O_2} < 0.1$ atm, the sample was oxidized at 1173 K and cooled to 873 K in 0.1 atm of oxygen. This was

to ensure the oxidation of the sample at low temperatures. As the authors assert, the estimated standard deviations of the reported values for oxygen stoichiometry are typically ±0.02. At the same time, their values for oxygen content are much lower than those reported earlier based on TG measurements [31, 32]. Respective data are shown in Fig. 4a for comparison. It is seen that the data derived from TGA measurements by different authors closely coincide, while the values obtained from in situ neutron diffraction are substantially smaller, the deviation increasing with temperature. Greater reliability of TGA data is also confirmed by reasonable values of oxygen content that correspond to the average oxidation degree of B cations larger than 3+. It agrees well with other works showing that the average oxidation degree of cobalt in air exceeds 3+ even at 1000 °C [3, 33], and the oxidation degree of iron greater than 3+ persists also at low oxygen activity [34, 35]. Controversially,
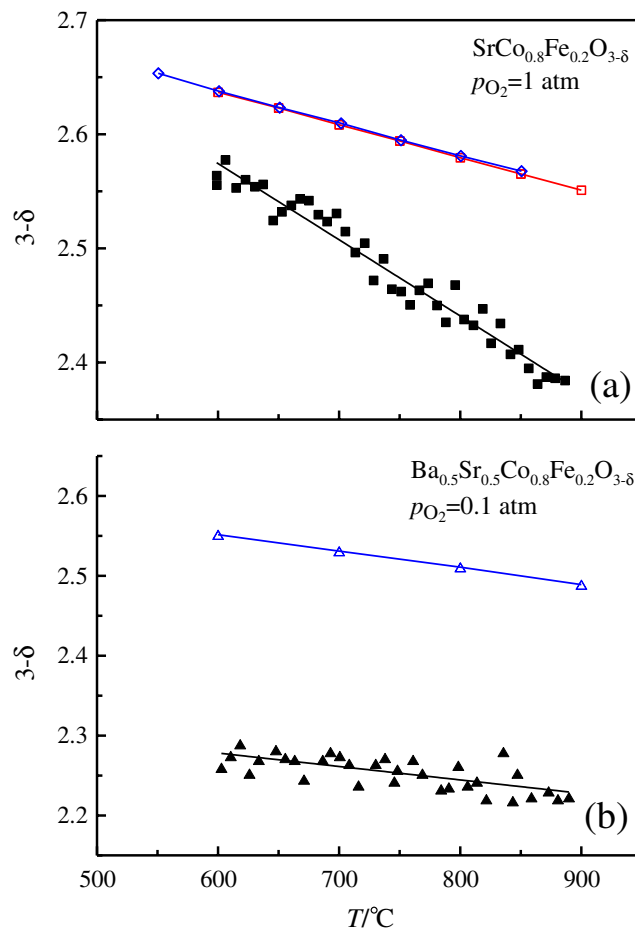

Fig. 4 a The temperature dependence of oxygen non-stoichiometry in $SrCo_{0.8}Fe_{0.2}O_{3-\delta}$ at $p_{O_2} = 1$ atm as obtained from thermogravimetric measurements (*open diamond*) [31] and (*open square*) [32] and in situ neutron powder diffraction (*filled square*) [30]. b The temperature dependence of oxygen non-stoichiometry in $Ba_{0.5}Sr_{0.5}Co_{0.8}Fe_{0.2}O_{3-\delta}$ at $p_{O_2} = 0.1$ atm as obtained from thermogravimetric measurements (*open triangle*) [38] and in situ neutron powder diffraction (*filled triangle*) [36]

NPD data [30] suggest that the average oxidation degree of iron or cobalt is smaller than 3+. Notice also [36] where oxygen content in $Ba_{0.5}Sr_{0.5}Co_{0.8}Fe_{0.2}O_{3-\delta}$ was studied with in situ neutron diffraction at p_{O_2} between 10^{-3} and 1 atm. Even in an oxygen atmosphere and at quite moderate heating to 730 °C, the obtained value for $3-\delta$ did not exceed 2.3, thus giving 40% of 2+ cations in the B sub-lattice. At the same time, high-temperature X-ray absorption in situ measurements in air directly demonstrate 3+ oxidation state of B cations in $Ba_{0.5}Sr_{0.5}Co_{0.8}Fe_{0.2}O_{3-\delta}$ at temperatures between 300 and 1233 K [37]. The NPD results at $p_{O_2} =$ 0.1 atm are shown in Fig. 4b together with TGA data [38] for comparison. Again, one can see a far too low oxygen content obtained from neutron diffraction.

On the other hand, the oxygen content determined from neutron diffraction for the brownmillerite phase $SrCo_{0.8}Fe_{0.2}$ $O_{3-\delta}$ occurs in good agreement with the value $3-\delta=2.5$ characteristic of brownmillerites, and strong disagreement between TGA and NPD data is peculiar to the cubic structure only. Similar disagreements are observed also between X-ray diffraction and high-resolution electron microscopy data in studies of $SrFe_{1-x}V_xO_{3-\delta}$ and $SrFe_{1-x}Nb_xO_{3-\delta}$ [39, 40]. Probably, the divergence is due to the fact that oxygen vacancies in oxides are not always random and tend to form small locally ordered clusters in the structure. When the size of the clusters is smaller than the length of neutron-coherent scattering (~2000 Å), the diffraction pattern reflects an average occupation of oxygen sites. As is pointed out in [29], this is the reason for the underestimation of oxygen occupancy and of oxygen content in oxides in NPD studies. The authors of [41] also suggested local defect clusters based on the observation of unusually large isotropic thermal parameters of oxygen in their analysis of oxygen-deficient oxides at high temperatures.

An instructive application of neutron diffraction for oxygen content measurements in a complex oxide was demonstrated in [42], where the occupation of oxygen sites in $Sr_3Fe_2O_{6+\delta}$ was examined as a function of temperature. The crystal structure of $Sr_3Fe_2O_{6+\delta}$, which is a member of the Ruddlesden–Popper $A_{n+1}B_nO_{3n+1}$ series, is formed by double perovskite layers $SrFeO_3$ alternating along the c axis with the SrO layers having the rock salt structure [43]. There are three non-equivalent oxygen sites in the structure (Fig. 5). Oxygen non-stoichiometry index δ in $Sr_3Fe_2O_{6+\delta}$ can vary as a function of temperature and oxygen pressure from 0 to 1. According to [43], oxygen vacancies mostly reside on O1 sites. Moreover, high-temperature transport properties [44] and structure refinement [45] both suggest vacancies on O3 sites. Results [42] in Fig. 6b, c show that the occupation of O1 and O3 sites decreases at heating, while O2 sites remain filled even at 900 °C. The obtained oxygen content variations with temperature are shown in Fig. 6a together with TGA [46] and coulometric titration
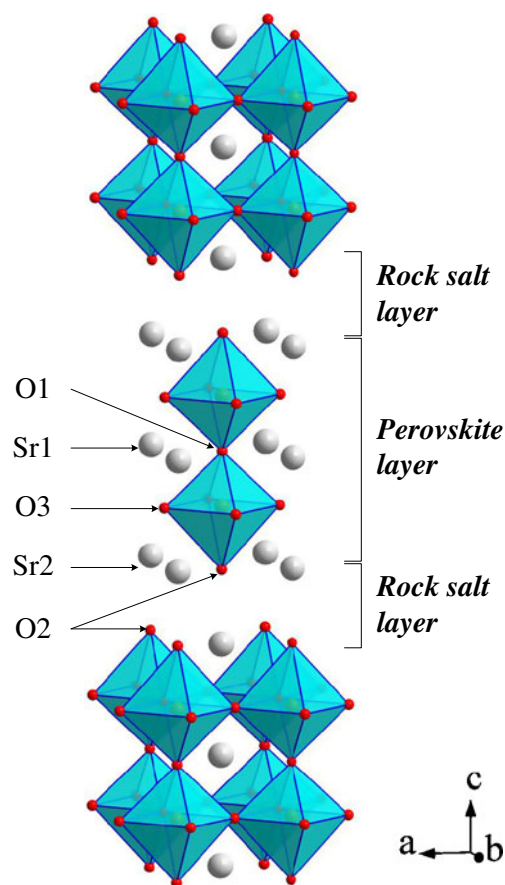

Fig. 5 The unit cell of $Sr_3Fe_2O_{6+\delta}$

data [47]. Although in situ neutron diffraction shows somewhat low values, the general trends and coincidence with other data seem satisfactory.

Substituted derivatives $Sr_3FeMO_{6+\delta}(M = Fe, Co, Ni)$ were studied in [48] with the use of neutron diffraction. The oxygen content in the samples was determined from the data recorded in air at $T=20, 300, 500, 700,$ and 900 °C. The results obtained at high temperatures agree with [42, 43] and clearly locate most of the oxygen vacancies on O1 sites. For instance, the vacancy concentration on O1 sites at 900 °C achieves 55%, 48%, and 57% in $Sr_3Fe_2O_{6+\delta}$, $Sr_3FeCoO_{6+\delta}$, and $Sr_3FeNiO_{6+\delta}$, respectively. The O2 sites in the rock salt layer were found invariably filled. The interesting feature is the presence of an appreciable amount of vacancies on O3 sites in $(Fe/M)O_2$ planes of the perovskite layers even when $\delta>0$ as it occurs in the parent ferrite $Sr_3Fe_2O_{6+\delta}$ [42].

Summarizing, it should be pointed out that, although NPD is less widely used at present than, e.g., TG measurements, the application of this technique to studies of oxides tends to increase. This can be explained by improvement of experimental approaches and computational methods for data acquisition and treatment and by inherent advantages. Unlike any other one, this method allows the determination
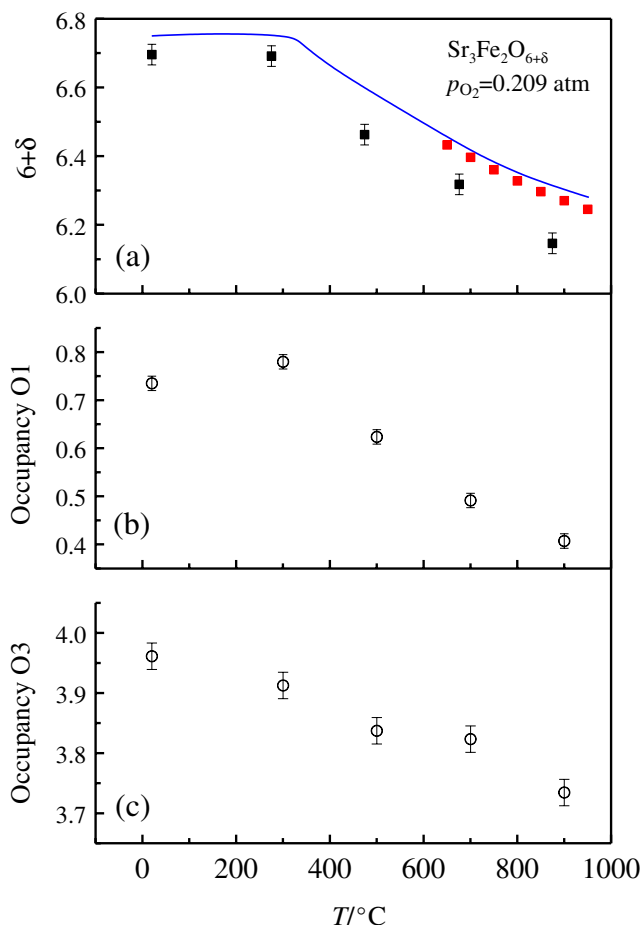
Fig. 6 The temperature dependence of oxygen content in $Sr_3Fe_2O_{6+\delta}$ in air as obtained from **a** thermogravimetric measurements (*solid line*) [46], coulometric titration (*colored filled square*) [47], and in situ neutron powder diffraction (*black filled square*) [42]; **b** O1 occupancy; **c** O3 occupancy [42]

Coulometric titration

Coulometric titration is based on measurements of chemical potential of oxygen in a gaseous phase, which is in thermodynamic equilibrium with the oxide sample under study. In a classical implementation of the method, a sample is placed into a sealed measuring cell that is equipped with one or two electrochemical elements for oxygen sensing and pumping. In the majority of cases, YSZ is used as a solid electrolyte for electrochemical elements. Current $I(t)$ passing through electrodes of electrochemical element during the interval of time $(t''-t')$ leads, according

to the Faraday law, to a variation in the amount of oxygen Δn_F in the inner volume of the cell

$$\Delta n_F = \frac{1}{2F} \int_{t'}^{t''} I(t) dt \tag{4}$$

Here, F is the Faraday constant. The passage of oxygen current results in a respective variation in the amount of oxygen (and accordingly pressure) in the gaseous phase in the cell

$$\Delta n_g = \frac{V}{R} \frac{\Delta p_{O_2}}{T} \tag{5}$$

and in the sample

$$\Delta n_s = \Delta n_F - 2\Delta n_g \tag{6}$$

Assuming an applicability of the ideal gas laws, the stoichiometry change can be expressed as

$$\Delta \delta = \frac{M_s}{m_s} \left(\frac{1}{2F} \int_{t'}^{t''} I(t) dt - 2\frac{V}{R} \left(\frac{p''_{O_2}}{T''} - \frac{p'_{O_2}}{T'} \right) \right) \tag{7}$$

where R is the gas constant, V is the cell free volume, and p'_{O_2}, T' and p''_{O_2}, T'' denote the pressure and absolute temperature in the initial and final state of the cell, respectively. Oxygen partial pressure inside the cell p_{O_2} can be determined in accordance with the Nernst equation by measuring the potential of the cell internal electrode relative to the reference electrode.

$$E = \frac{RT}{4F} \ln \left(\frac{p_{O_2}}{p_{O_2}^{ref}} \right) \tag{8}$$

In most cases, the reference electrode is in air during measurements, i.e., $p_{O_2}^{ref} = 0.209$ atm. The sensitivity of the method is basically determined by the baric contribution to Eq. 7 and can be estimated considering the measurement accuracy $\sim 10^{-5}$ V of modern voltmeters. Using Eq. 8, it is possible to calculate the corresponding variation of oxygen pressure and then to determine the change in the amount of oxygen in the cell internal volume. If we assume $V=1$ cm^3 and $T=1000$ K for estimation, it is readily seen that the resolution of the method is $\sim 10^{-8}$ mol O_2, which is two orders of magnitude higher than the typical sensitivity of the gravimetric method (10^{-5} g or $\sim 10^{-6}$ mol O_2). The unique feature of coulometric titration is that measurements can be carried out at very small activities of oxygen in gaseous phase. The additional merit is the comparatively inexpensive experimental equipment, which requires only a voltmeter and a current source. Since data acquisition consists in electric measurements, the experiment can be easily computerized, which is very important for prolonged runs. Despite the high accuracy, coulometric titration is not used so widely as, e.g., thermo-gravimetric method. Apparently, this is largely due to

not only of total oxygen content but also of oxygen distribution over non-equivalent crystallographic sites. This feature makes neutron diffraction particularly valuable for studies of oxides with a complicated crystal structure.

operation simplicity and availability of commercial TGA equipment.

Coulometric titration errors

The total error of the method Er_{CT} reflects influence of a number of factors

$$Er_{CT} = Er_F + Er_V + Er_{eq} + Er_{YSZ} + Er_l \qquad (9)$$

Here, Er_F is the integration error due to inaccuracy in measurements of the charge passing through the oxygen pump during titration, Er_V is the error related to determination of the cell free volume, Er_{eq} is the error caused by the deviation of the system from equilibrium, Er_{YSZ} is the error due to oxygen non-stoichiometry of the electrolyte, and Er_l is the contribution from uncontrolled leaks of oxygen into the measuring cell due to cracks, pores, and marginal electron conductivity. The terms in Eq. 9 are defined as the ratio between the corresponding contribution $\Delta\delta_i$ and the variation in the total oxygen content in the sample $\Delta\delta$, $Er_i = \Delta\delta_i / \Delta\delta$. The contributions to Er_{CT} versus oxygen pressure are shown in Fig. 7.

Er_F, which is due to current determination inaccuracy, depends on the stability of the current source, metering device errors, measurement frequency, and the inaccuracy in determination of the integration time. The uncertainty of the latter value may be due to the response time of current source. Therefore, the error may be reduced by increasing the time of titration. Generally, the current integration error

changes the slope of the isotherm while not affecting the measurement reversibility (Fig. 7a). The typical value of Er_F during measurements is not greater than 0.1% [49].

The contribution Er_V can be estimated by comparing the amount of oxygen in the cell free volume and the amount of oxygen taken in or released by the sample. The free volume of a small cell ($V \sim 1$ ml) can be determined with an accuracy of ± 0.01 ml by filling the cell with alcohol. Figure 7b shows a titration isotherm for 0.187 g of $La_{0.8}Sr_{0.2}FeO_{3-\delta}$ and how it changes when an error enters determination of the free volume. As is seen, disregarding the free volume or an error in its determination both result in significant deviations from correct values at $p_{O_2} > 10^{-2}$ atm. It is clear that the errors will decrease as the oxide homogeneity region and the sample mass increase, and the errors will become more pronounced with an increase in free volume. Sometimes, it is difficult to measure the free volume of the cell because of its complicated geometry. Moreover, this information becomes insufficient when the free volume is not kept in isothermal conditions. In such cases, the upper pressure limit is chosen so that the estimation of the error on the basis of Eq. 7 meets the requirements of the experimental task. For example, in works [50–53] where a measuring cell with non-isothermal free volume was used, measurements were performed at $p_{O_2} < 10^{-4}$ atm neglecting the contribution from the free volume, and the error in non-stoichiometry determination being less than 0.1%. The effect of the free volume is not exhausted by the contribution to the measurement errors. According to Eq. 5, the variation in

Fig. 7 The influence of oxygen pressure upon different contributions (see text) to coulometric titration isotherms for perovskite-like ferrites at 900 °C. Empty and filled symbols show data obtained at in-pumping followed by out-pumping of oxygen, respectively
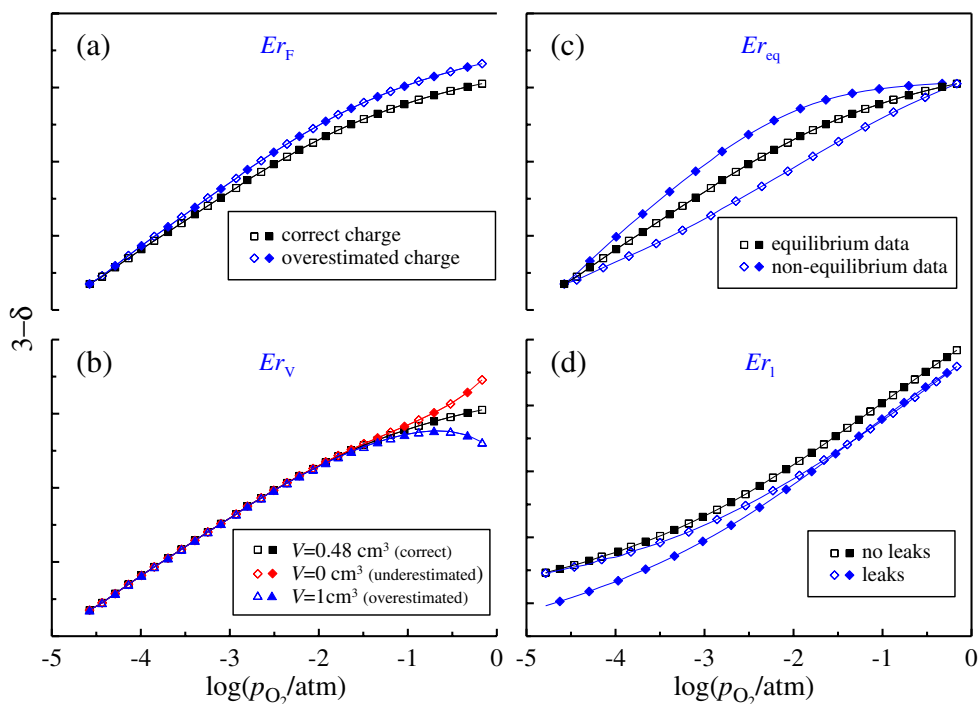
pressure with a change in oxygen content in the cell is inversely proportional to the cell free volume. Since the pressure relaxation rate is determined by the degree of deviation from the equilibrium state, reduction in the free volume promotes a decrease of the duration of measurements.

Temperature change and current passage through an oxygen pump both disturb the equilibrium of the sample with the gaseous phase. As a result of oxygen exchange between the sample and the gaseous phase, the relaxation of the cell to a new equilibrium state begins. This process may last from several minutes to tens of hours, and its completion is judged from the fulfillment of a pre-chosen equilibrium criterion. For example, in [54], a change of the sensor e.m.f. less than 0.2±0.3 mV/min was taken as equilibrium criterion. In [55], the equilibrium criterion was the change in oxygen sensor potential at less than 0.1%/min. The equilibrium criterion must be chosen in such a manner that the error Er_{eq} caused by a deviation from the equilibrium state is minimal. Relevant control is provided by successive measurements in the mode when the oxygen pressure or temperature decreases and then increases backward to initial values. A characteristic feature showing that equilibrium was not achieved during measurements is hysteresis (Fig. 7c). Since diffusion and surface exchange become sluggish with temperature decrease, the error due to deviation from equilibrium may be higher at low temperatures. However, when the deviation from equilibrium is due to a phase transition, the value of hysteresis may even decrease with temperature [56].

The error due to electrochemical leak caused by oxygen non-stoichiometry of electrolyte Er_{YSZ} may distort measurement results if the oxide under studies has a small oxygen homogeneity region, which is comparable with that in YSZ. Thus, it is shown that oxygen non-stoichiometry variations in $BaTiO_{3-\delta}$, $SrTiO_{3-\delta}$, and YSZ are comparable [57, 58]. In order to reduce Er_{YSZ}, the authors used a large mass of the sample (about 16 g) and decreased the mass of the electrolyte to 0.7 g. This measure allowed them to decrease the error caused by YSZ non-stoichiometry to 3%.

The error due to uncontrolled oxygen leaks Er_l manifests itself in irreversibility of measurement results (Fig. 7d). Since in most cases leaks have the greatest impact upon results of titration, they should be considered in more detail.

The problem of electrochemical oxygen leaks

Under oxygen pressure gradient, uncontrolled oxygen leaks into the measuring cell may be a consequence of pores and microcracks in the cell walls and in the sealing material. However, the most significant contribution is made by oxygen leaks that result from the small electronic conductivity of the electrolyte. The ionic σ_i and electronic, n-type σ_n and p-type σ_p, components of conductivity for the most extensively used 8 mol.% YSZ electrolyte are represented [59] as

$$\sigma_i = 1.63 \ 10^2 \exp\left(-\frac{0.79 \text{ eV}}{kT}\right) \tag{10}$$

$$\sigma_n = 1.31 \ 10^7 \exp\left(-\frac{3.88 \text{ eV}}{kT}\right) p_{O_2}^{-1/4} \tag{11}$$

$$\sigma_p = 2.35 \ 10^2 \exp\left(-\frac{1.67 \text{ eV}}{kT}\right) p_{O_2}^{+1/4} \tag{12}$$

Using these data, it is possible to calculate ambipolar conductivity

$$\sigma_{am} = \frac{\sigma_i(\sigma_n + \sigma_p)}{\sigma_i + \sigma_n + \sigma_p} \tag{13}$$

which determines oxygen ion current through the electrolyte because of the inner short circuit when oxygen pressure gradient is applied. The corresponding data are presented in Fig. 8a. It is seen that the ambipolar conductivity of electrolyte at 600 °C does not exceed 10^{-7} S cm^{-1} in the widest range of oxygen partial pressure, and therefore the respective error in most cases may be neglected. However, ambipolar conductivity increases significantly with temperature. In order to estimate the emerging error, one can consider a measuring cell with a wall thickness of l=0.1 cm and surface area of s=5 cm^2 as an example. The amount of oxygen permeating the cell can be calculated using the known relationship [60]

$$jo_2 = \frac{RT}{16F^2} \frac{s}{l} \int_{p_{O_2}^{ref}}^{p_{O_2}} \sigma_{amb}(p_{O_2}) \text{d} \ln p_{O_2} \tag{14}$$

Figure 8b displays the calculation results. It is seen that the 10^{-2} μmol resolution can be achieved only at temperatures below 700 °C. At higher temperatures, the error will be larger. Better accuracy is attained by special arrangement of measurements and by correction of the obtained results with allowance for leaks rate.

Minimization of electrochemical leak rate

The basic methods for leaks rate minimization follow from Eq. 14, and they include:

Reduction of electrolyte area Generally, the minimal area of an electrolyte is determined by the required yield of the oxygen pump at the minimal temperature of the experiment. It is easy to estimate from Eq. 10 that an YSZ pump with
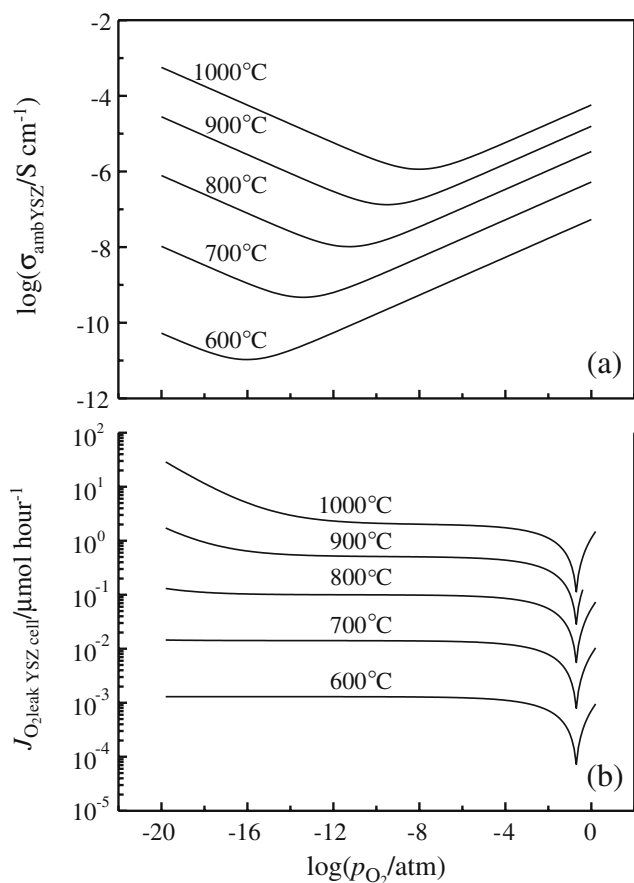
Fig. 8 **a** The ambipolar conductivity in YSZ as a function of partial pressure of oxygen at different temperatures as calculated from Eqs. 10–13. **b** The oxygen leaks in YSZ cell as a function of oxygen partial pressure in the cell. The cell wall thickness of 1 mm and surface area of 5 cm^2 are used in calculations according to Eqs. 13 and 14. The cell outer atmosphere is air

the area of 1 cm^2 and wall thickness of 1 mm provides a current of ~45 mA at 600 °C and voltage 1 V. Since typical titration currents vary within 5–500 μA [57], 0.5–0.8 mA [61], and 5–15 mA [54], this area is sufficient for the electrochemical element. In most cases, the measuring cell is made completely of electrolyte to circumvent the difficulties associated with the incompatibility of thermal expansion coefficients when heterogeneous materials are used [49, 62, 63]. If an extremely high accuracy is required, the cell is made of alumina, which is impermeable for oxygen, while the electrochemical element is used as a cell cover [55–58].

Optimization of measurement duration In order to reach equilibrium between the sample and the gaseous phase in the cell, it is required that oxygen transport in the sample takes place more quickly than when the oxygen content in the cell changes because of the leaks. This requirement is a fundamental restriction in the choice of materials to be studied with coulometric titration. Since equilibration of the

sample and the gaseous phase may take a considerable time and oxygen exchange and diffusion slow down as the cell approaches equilibrium, it is desirable to use a finely powdered sample. Besides, the equilibrium criterion should be chosen such that the error occurring as a result of leaks or deviations from equilibrium is minimal. In some cases, it is possible to accelerate the equilibration by a direct supply of oxygen from electrolyte to the oxide as was done in [50–53], because at such arrangement oxygen ions are transferred directly to the specimen, bypassing the gas phase.

Increase in sample mass It is clear that, if the sample mass is increased with the leaks rate value being constant, the error will decrease as much. Depending on a specific experimental implementation, the differences in the sample mass may reach three orders of magnitude from 0.08 to 16 g [53, 54, 57, 61].

Decrease in oxygen partial pressure gradient The use of air at the outer side of the measuring cell as the atmosphere for the reference electrode is most widely utilized because it provides reliable $p_{O_2}^{ref}$ values for the determination of oxygen partial pressure inside the measuring cell and simplifies the design. However, a large oxygen gradient over electrolyte during measurements results in considerable leaks. Leak rate may be decreased if a special gaseous mixture is used at the outer side of the measuring cell so that the motive force for the leaks is reduced over the whole experimental pressure interval. Thus, oxygen non-stoichiometry in iron–magnesium spinel was examined in the range $10^{-8} < p_{O_2}/atm < 10^{-2}$ in [64] where the outer side of the cell was in nitrogen atmosphere $\left(p_{O_2}^{ref} \sim 10^{-4} \text{ atm} \right)$. The oxygen non-stoichiometry in barium titanate was studied in the range $10^{-12} < p_{O_2}/atm < 10^{-2}$ in [57] where mixtures CO_2/CO with gas ratio from 30:1 to 15:1 were used. Developing this approach, the authors of [65] suggested a measuring system where oxygen activity at the outer side of the measuring cell was maintained with the help of vacuum equipment (pumps, manometers, stopcocks) and an electrochemical sensor, which permitted the smooth change of the total gas pressure and oxygen activity. The system made it possible to maintain the minimal oxygen gradient across the cell over a wide pressure range and thereby to substantially reduce the leak rate. Later, [66] used an electrochemical pump in place of a mechanical one to maintain the minimal oxygen gradient and make the measuring system compact and easy in operation.

Evaluation of leak rate

The methods described in "Minimization of electrochemical leak rate" allow only the reduction of the leak rate but do not completely prevent the process. Therefore, an valuation

of the magnitude of leaks is an important task. The authors of [49, 67] used measuring cells of very small volume (0.15–0.25 ml), and before performing the measurements they tested the blank cells in order to determine the leak rate. It can be seen from Fig. 9 that the leak current does not exceed 250 nA as defined by the authors from the plot $\log(p_{O_2}/\text{atm})$ vs. time. Therefore, the leaks cannot have a noticeable effect on the titration results and can be neglected. It should be noted that the measuring cells in this study were tested at 933 and 978 K, while the measurements are usually performed at temperatures up to 1223 K. The higher temperatures lead to the increase in leak rate to about two orders of magnitude (Fig. 8b).

In order to avoid significant errors, the measured results are to be corrected with allowance for electrochemical leaks. For this purpose, it is necessary to calculate the ambipolar conductivity according to Eqs. 10–13 (Fig. 8a). In order to obtain an analytical expression, [55, 56] neglected the ionic contribution and corrected their results by making use of a simplified equation

$$J_O = \frac{RT}{Fl} \times \left[\sigma_p\left(p_{O_2}^{\text{ref}}\right) \times \left\{ \left(\frac{p_{O_2}}{p_{O_2}^{\text{ref}}}\right)^{0.25} - 1 \right\} + \sigma_n\left(p_{O_2}^{\text{ref}}\right) \times \left\{ 1 - \left(\frac{p_{O_2}}{p_{O_2}^{\text{ref}}}\right)^{-0.25} \right\} \right] \quad (15)$$

The data for σ_p and σ_n were taken from [59]. This approximation is quite justified for rather wide temperature and oxygen pressure limits; the more so since it is exactly on the basis of this expression that [59] determined the electronic contribution to conductivity in YSZ. Note, however, that with this approach it is impossible to control leaks through cracks, pores, and defects in the cell and seals.

In [68], three independent methods for leak determination $[(\mathrm{d}\Delta\delta)\mathrm{d}t]_{\text{leak}}$ were used in order to characterize the YSZ cell.

a. The $[(\mathrm{d}p_{O_2})/\mathrm{d}t]_{\text{empty}}$ of an empty titration cell (no sample) was measured at various p_{O_2} values and temperatures over an extended period of time. The pressure was transformed to the number of moles (n_{O_2}) using the ideal gas law, $[(\mathrm{d}n_{O_2})/\mathrm{d}t]_{\text{empty}}$, and finally expressed as $[(\mathrm{d}\Delta\delta)/\mathrm{d}t]_{\text{leak}}$, assuming that the change in oxygen content originates from a change in δ of an equal amount of sample as in the filled cup. The leak rate estimated in this way was of the order of 10^{-32}, 10^{-19}, and 10^{-9} s^{-1} at 600, 700, and 800 °C, respectively, indicative of a very good seal.

b. The difference in pumped charge over an isothermal titration cycle was determined, and a mean leak rate was obtained from

$$\overline{\left(\frac{\mathrm{d}\Delta\delta}{\mathrm{d}t}\right)}_{\text{leak}} = \frac{Q_{\text{out}} - Q_{\text{in}}}{2Fnt} \quad (16)$$

where Q_{out} is the total charge needed to be pumped to reach the lowest p_{O_2} value of the titration cycle, Q_{in} is the total charge that has to be pumped to return to the starting point in p_{O_2}, n is the amount of powder in the titration cell expressed in moles, and t is the duration of the titration cycle. Leak rates determined by this method were of the order of 10^{-10}–10^{-8} s^{-1} between 600 and 900 °C [68]. The advantage of this method is that the leak rate is determined during regular measurements, i.e., it does not require extra time. The drawback is the leak rate value averaged over oxygen pressure interval, whereas at the limiting points of the examined p_{O_2} range the leaks may differ not only in rate but even in direction.

c. The $[(\mathrm{d}p_{O_2})/\mathrm{d}t]_{\text{filled}}$ of the loaded titration cell was measured at steady state, and the leak rate was estimated from

$$\left(\frac{\mathrm{d}\Delta\delta}{\mathrm{d}t}\right)_{\text{leak}} = \left(\frac{\mathrm{d}p_{O_2}}{\mathrm{d}t}\right)_{\text{filled}} \left(\frac{\mathrm{d}\Delta\delta}{\mathrm{d}p_{O_2}}\right)_{\text{filled}} \quad (17)$$
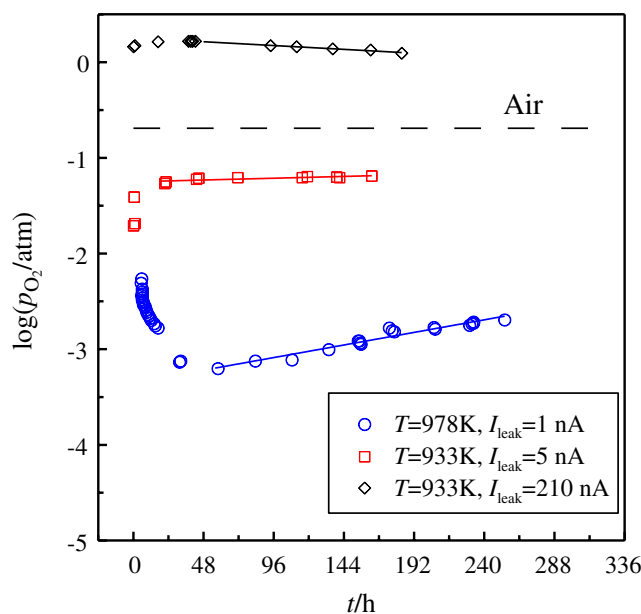

Fig. 9 The oxygen partial pressure changes caused by leaks in the empty measuring cells. *Solid lines* correspond to oxygen leaks as calculated for leak currents in the legend [49]

This approach allowed the estimation of the variation in the leak rate over time. The estimations of the leak rate in this manner were practically identical to the mean leak rate obtained by method B without a significant variation over time [68]. This method permits a very accurate determination of leak rate but requires a considerable time.

It was shown [69] that under isothermal conditions the leak rate may be considered by an approximation of experimental values with the relationship

$$I_{leak} = \alpha \left[\left(p_{O_2}^{ref} \right)^{\frac{1}{4}} - \left(p_{O_2} \right)^{\frac{1}{4}} \right] \qquad (18)$$

where α is a constant determined experimentally by choosing such a titration current that the p_{O_2} value remains constant with time. This method is convenient because it is sufficient to determine experimentally the α value for each operation temperature before measurements. The limitation of the method is that Eq. 18 allows consideration of only the electrochemical leak rate, as is the case with Eq. 15.

Measurement techniques

In general, oxygen coulometric titration measurements can be performed either by monitoring the e.m.f. response to a d.c. current pulse of known duration (*galvanostatic method*) or by monitoring the current decay after a stepwise change in the e.m.f. (*potentiostatic method*). In view of Eq. 8, a potentiostatic step involves a change in oxygen partial pressure inside the cell. Chemical diffusion allows the sample to adapt its stoichiometry to the newly adjusted p_{O_2}. The rate of equilibration is monitored by measuring the current, which decays over time toward a minimum value. The latter is due to the unavoidable leak current, I_{leak}, and is determined by the quality of the glass sealing and the nonvanishing electronic conductivity of the zirconia electrolyte [70]. When oxygen content changes in the gas phase over the sample can be ignored, $\Delta\delta$ is determined as

$$\Delta\delta = \frac{M_s}{m_s} \frac{1}{2F} \int_{t=0}^{t=\infty} (I(t) - I_{leak}) dt \qquad (19)$$

For non-stoichiometric oxides, application of the potentiostatic step mode has some advantages over the galvanostatic method, which include: (1) easy determination of the leak current and (2) at the end of the current decay, the cell is in a steady state because p_{O_2} is fixed by the imposed e.m.f. On the contrary, at the end of a galvanostatic pulse, the oxygen partial pressure drifts back to that of the ambient value by leaks of oxygen [70]. The titration method in the potentiostatic mode is particularly effective for measurements at high temperatures and high oxygen pressure gradients, when I_{leak} is big enough to be measured with high accuracy. The drawback of the method is the insufficiently rigorous consideration of the leak rate since it changes in the process of pressure relaxation and has a complicated time-dependent profile.

Along with the abovementioned methods, the temperature step method is often used which allows an accurate determination of the thermodynamic quantities. As the gas inside the cell contains only a very small amount of oxygen, δ is constant during such a temperature cycle. This has the advantages that partial molar entropy $\overline{S_O} = -(\partial\mu_O/\partial T)_\delta$ and partial molar enthalpy of oxidation $\overline{H_O} = (\partial(\mu_O/T)/\partial(1/T))_\delta$ can be easily evaluated and also that only minute amounts of oxygen are needed to be exchanged to obtain equilibrium between the gas and the powder, thus resulting in fast equilibration [71, 72]

Determination of oxygen stoichiometry in starting materials

The considered methods allow only measurements of changes $\Delta\delta(p_{O_2}, T)$ in the oxygen content in the sample when ambient gas thermodynamic parameters change. To determine the absolute content of oxygen, additional methods should be applied, which permit establishing the correspondence between the obtained data array and the absolute values of $\Delta\delta(p_{O_2}, T)$. The simplest technique for oxygen content determination in oxides is synthesis from well-defined starting reagents with a control of the mass of the reaction product. However, the obtainment of a single phase final product usually involves several intermediate grindings, which lead to the accumulation of weighing errors. Sometimes, the stable state of oxide under certain conditions is used as the reference composition. For example, the authors of [73] report that δ value in air at room temperature is zero in $La_{1-x}Ca_xCrO_{3-\delta}$ with x up to 0.7. Iodometric titration is also often used for the determination of oxygen content in oxides [21, 25, 53, 74]. Since many cations in oxides can be reduced to metallic state during heating in hydrogen, the absolute content of oxygen in these oxides can be determined by reduction with continuous mass monitoring in hydrogen-containing gaseous mixtures. Knowing the mass loss, it is possible to calculate the absolute content of oxygen in the oxide before reduction [49, 53, 67].

If an oxide has a wide forbidden gap and the disproportionation reactions have no noticeable effects, the absolute content of oxygen can be determined from analysis of isothermal dependences $\Delta\delta = f(p_{O_2})$. The isotherm has an inflection point corresponding to the integral charge of a certain cation in the structure [75, 76]. Determination of the absolute oxygen content in $La_{0.2}Sr_{0.8}Fe_{0.55}Ti_{0.45}O_{3-\delta}$ is shown as an example

in Fig. 10(a) [77]. For $La_{0.2}^{3+}Sr_{0.8}^{2+}Fe_{0.55}^{3+}Ti_{0.45}^{4+}O_{3-\delta}$, an inflection in the titration data is indicative of $\delta = 0.175$. The solid line in this plot is $\partial\delta/\partial p_{O_2}$. The state in which iron atoms have an average oxidation degree 3+ corresponds to the minimum concentration of electrons (Fe^{2+}) and holes (Fe^{4+}). Conductivity in this state exhibits a minimum if mobility values for electrons and holes are equal. The behavior of the conduction curve may be indicative of a certain oxidation degree and therefore it may be used for the determination of the absolute oxygen content. Figure 10b shows the isotherms of oxygen content and conductivity in $SrFe_{0.9}Al_{0.1}O_{3-\delta}$ as an example of the absolute oxygen content determination [78].

In [57], the absolute oxygen content in barium titanate was determined on the basis of defect structure analysis and approximation of the experimental data. Since the oxygen homogeneity range in $BaTiO_{3-\delta}$ is very narrow ($\delta \sim 10^{-4}$), even a small amount of acceptor impurity may have a considerable effect on the position of the stoichiometry point. The authors of [57] derived an expression from their defect model, which enabled the description of experimental data (Fig. 11) and determination of the ionization constant K_i, oxygen pressure $p_{O_2}^0$ for stoichiometric state,

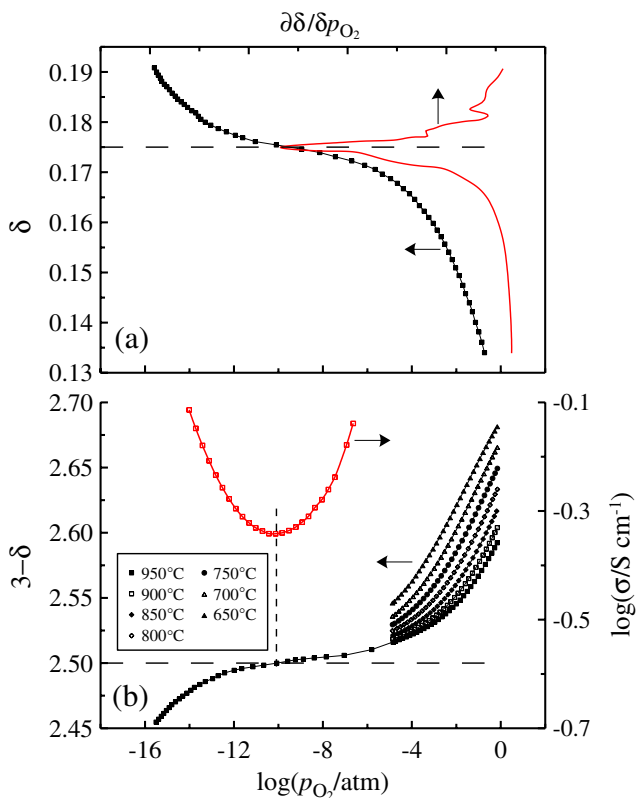**Fig. 11** The plots of δ vs. $\log(p_{O_2}/atm)$ for $BaTiO_{3-\delta}$ at different temperatures. *Solid lines* show the best fitting of experimental data with Eq. 20 [57]

and a correction for deviations of titration results from the stoichiometric state δ^*

$$\Delta\delta = \delta - \delta^* = -\frac{V_m}{N_A}\sqrt{K_i}\left[\frac{1}{4}\ln\frac{p_{O_2}}{p_{O_2}^0}\right] - \delta^* \qquad (20)$$

Here, N_A and V_m denote the Avogadro's number and molar volume of $BaTiO_{3-\delta}$, respectively.

Experimental features

Coulometric titration was first used in the 1960s. Over this period, the method has undergone considerable improvements. In recent works, the measuring cells of a small internal volume are most often used, which equipped with one or two pairs of platinum electrodes and are made either entirely of YSZ or of YSZ and alumina. A considerable restriction in the application of such cells is that measurements cannot be performed at temperatures below 600 °C because of the poor conductivity of the electrolyte. Therefore, the important temperature range 350-400 °C occurs out of reach where intensive oxygen exchange with the gas phase develops in many oxides.

The technique employed in [79] allowed coulometric titration of $Bi_2V_{0.9}Cu_{0.1}O_{5.5-\delta}$ at 400 °C. Along with the usual small-sized titration cell (cell 1), an additional electrochemical cell of increased length (Cell 2) was used, which was in non-isothermal conditions during measurements (Fig. 12). The free internal volume of cell 1 was about 0.8 ml. The width of porous metal Pt electrodes was

Fig. 10 a Determination of stoichiometric composition in $La_{0.2}Sr_{0.8}Fe_{0.55}Ti_{0.45}O_{3-\delta}$ at the minimum value of $\partial\delta/\partial p_{O_2}$ at 950 °C [77]; **b** Determination of stoichiometric composition in $SrFe_{0.9}Al_{0.1}O_{3-\delta}$ at the minimum value of conductivity [78]

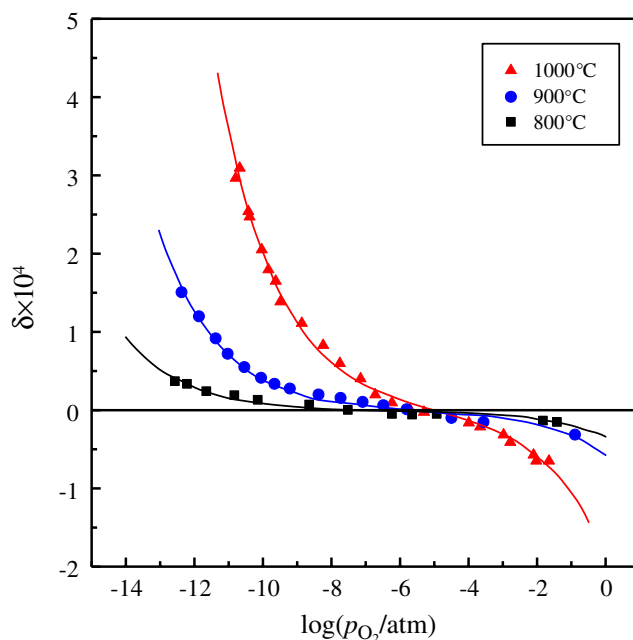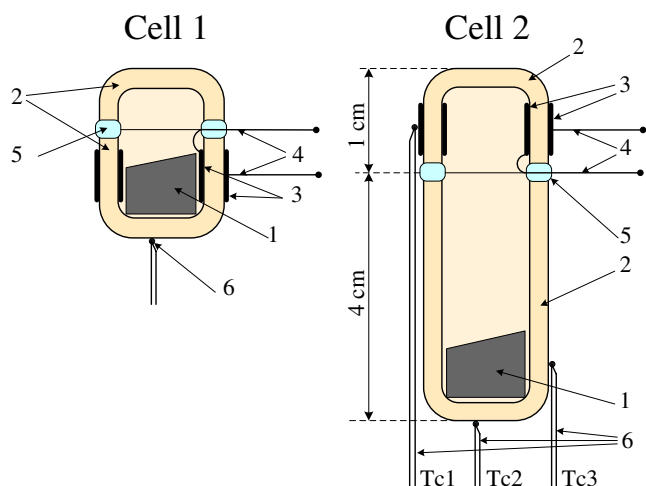**Fig. 12** Schematic drawing of coulometric cells used in [79]. *1*, porous sample; *2*, YSZ; *3*, porous Pt electrodes; *4*, platinum current collectors; *5*, glass–ceramic sealant; *6*, thermocouple

5–7 mm. In the case of cell 2, three thermocouples were used for temperature monitoring, Tc1, Tc2, and Tc3 (respective temperature values are T_1, T_2 and T_3). The measuring cells were placed in a two-zone furnace; the temperature of electrodes (T_1) varied in the range 820–1050 K. The sample temperature was measured with thermocouples Tc1 and Tc3. The difference in T_1 and T_2 was up to 150 K. Although the difference between T_2 and T_3 was less than 5 K, the sample temperature was taken average between these two thermocouples [79]. The results of measurements in non-isothermal conditions were processed assuming that the temperature change along the cell length was linear. The fact that the results obtained with using cell 1 and cell 2 closely coincide confirms the validity of this approach for non-isothermal measurements.

The authors of [50–53] used thermogravimetry and coulometric titration in the range $p_{O_2} \geq 10^{-5}$ atm and 10^{-4} atm $\leq p_{O_2}$, respectively. Thermogravimetry was not used at the lower pressures because of the slow rate of reaction between the gas phase and specimen, which resulted in exceedingly long time necessary for the equilibrium to be attained. Coulometric titration was not used at high pressures since analysis of the data was not simple in that range [51]. Note that this problem emerged solely due to the design characteristics of the electrochemical cell, Fig. 13. A slightly sintered sample of about 0.7 g was weighted and placed in at the closed end of YSZ tube having 5 mm inner diameter and 300 mm length. The sample was compressed to the end of the tube by means of a tubular silica pusher and spring. Pt mesh and Pt wire were used for the current collector from sample. Pt paste was applied to the outer wall of the tube as an air electrode. The cell was sealed with argon of about 0.1 atm at room temperature [50]. The utility of the cell is that it is sealed at

room temperatures. The special feature of the measurements is a rather large free volume of the cell in a complicated temperature field. Such a configuration makes it difficult to monitor oxygen content in the gas phase, but at the same time it provides direct passage of oxygen ions from electrolyte to the examined oxide bypassing intermediate transition to the gas phase and thus accelerating the measurements [53]. Coulometric titration was also used to determine the stability of oxides. When the extracted oxygen from the sample exceeded a certain amount, the equilibrium e.m.f. did not change with further extraction of oxygen. This indicated that the sample began to decompose. For the e.m.f., under this condition the decomposition p_{O_2} was determined [50]. The results of oxygen non-stoichiometry studies by the coulometric titration and the high temperature gravimetry in Fig. 14 demonstrate an excellent agreement [53].

To reduce the error due to electrochemical leaks, the authors of [57, 58, 64, 80, 81] developed a special design of the measuring cell. The small values of oxygen non-
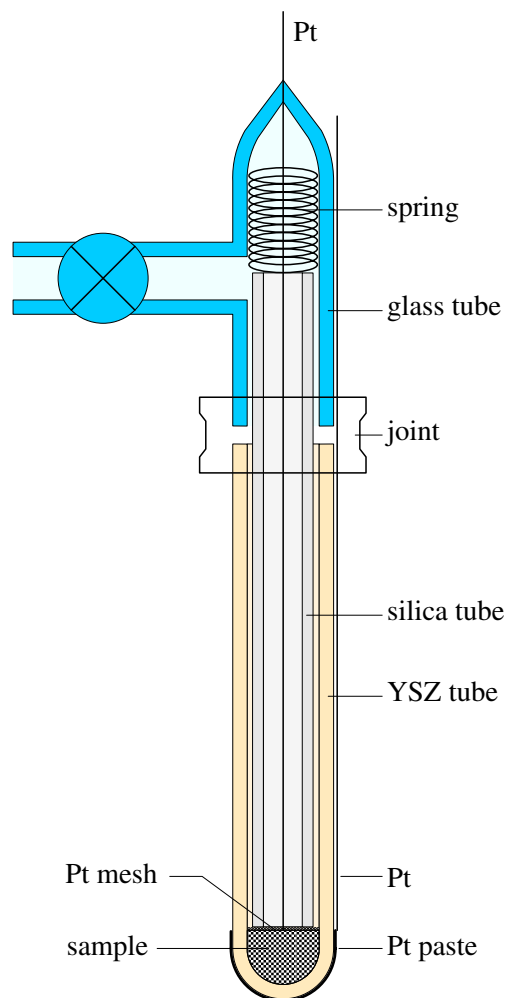

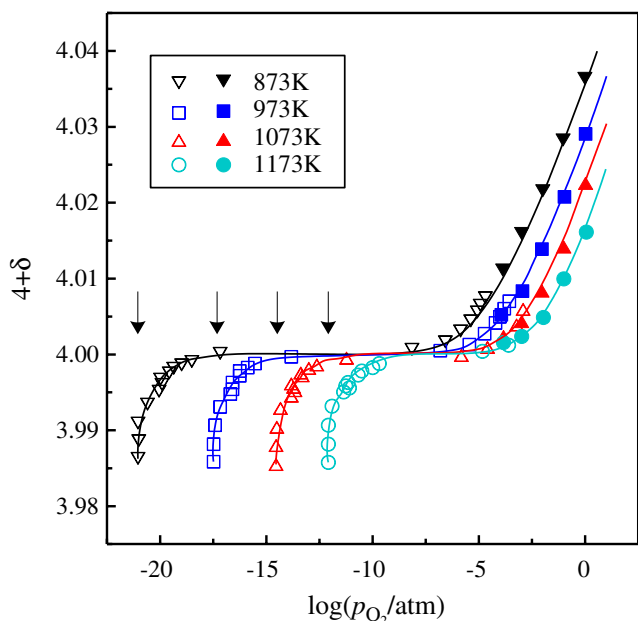**Fig. 13** Schematic drawing of the coulometric titration cell suggested in [50]

Fig. 14 Oxygen non-stoichiometry of $La_{1.8}Sr_{0.2}NiO_{4+\delta}$. *Open symbols* and *closed symbols* were measured by the coulometric titration and the high-temperature gravimetry, respectively. Decomposition pressures at different temperatures are shown by *arrows* [53]

stoichiometry in the studied oxides (TiO_2, Ba, and Sr titanates) impose particularly strict requirements to the experimental technique (Fig. 15). A small disk of YSZ was employed as a solid oxide electrolyte. Both planar surfaces of the disk were polished with diamond pastes of grit sizes down to 1 μm. A gas electrode was formed upon each side of the YSZ disk by attaching a round piece of platinum gauze with the aid of platinum paste and firing overnight at 1100 °C in air atmosphere. A platinum lead wire of 0.2-mm diameter was then attached to each of the gauze electrodes by firing similarly. An alumina cup was taken, and a hole of 5-mm diameter was drilled at the center of its closed bottom. The hole was hermetically sealed by the electrolyte with the aid of a gold ring as a sealing flange. The marginal space between the electrolyte and the cup bottom was filled with borosilicate glass powder. This glass-powder fill-up ensured a gastight seal by melting during titration operation at elevated temperatures. Specimen pellets were placed upon an alumina disk and covered by the alumina cup. In order to avoid any possible reaction between the specimen and bottom disk, a Pt foil was inserted in between. The inner lead wire was made by piercing through a shallow groove on the open-end rim of the cup. The authors of [57] employed an unusually large, 14–16 g, amount of $BaTiO_{3-\delta}$. It was because the non-stoichiometry changes in YSZ itself [82] are by no means negligible compared to that in $BaTiO_{3-\delta}$. The amount of $BaTiO_{3-\delta}$ was thus chosen in such a way that overall change in oxygen content of the sample itself would be at least an order of magnitude larger than in the YSZ-electrolyte (~0.7 g). The

as-assembled titration cell was put into an alumina crucible. The space between the cell and the crucible was completely filled with the glass powder, which would provide a perfect gas-tight seal at titration temperatures. The entire assembly was placed in a vertical furnace and fired up to a temperature of interest with a light spring pressure applied axially from above. Sample temperature was monitored with an S-type thermocouple, and the temperature of the electrolyte was corrected on the basis of the measured temperature profile of the furnace employed. The free cell volume was 0.3–2.2 cm^3, depending on the cells. At pressures above $10^{-2.5}$ atm, the change in oxygen content in the cell of such volume occurring with a pressure change by characteristic titration step $10^{-0.3}$ atm is comparable with that in a sample, and therefore the effect of free volume must be taken into consideration. With an analogous pressure step at about $10^{-3.6}$ atm, the change in the oxygen content in the free volume is two orders of magnitude smaller than that in the sample, and therefore the effect of free volume may be disregarded. The gas mixture CO/CO_2 was employed as $p_{O_2}^{ref}$ in order to suppress the electrochemical permeation through the YSZ electrolyte itself as much as possible. The experimental setup provided measurements of oxygen non-stoichiometry in $BaTiO_{3-\delta}$ with resolution $\Delta\delta \sim 10^{-6}–10^{-5}$ (Fig. 11). The work is interesting because the authors calculated the absolute oxygen content in $BaTiO_{3-\delta}$ on the basis of obtained experimental data, estimated the concentration of acceptor impurities in the material, and made an evaluation of measurement errors related to oxygen non-stoichiometry of the electrolyte.

The authors of [81] demonstrate a comparison of thermogravimetry and coulometric titration in their latest implementation. Oxygen non-stoichiometry in $TiO_{2-\delta}$ was
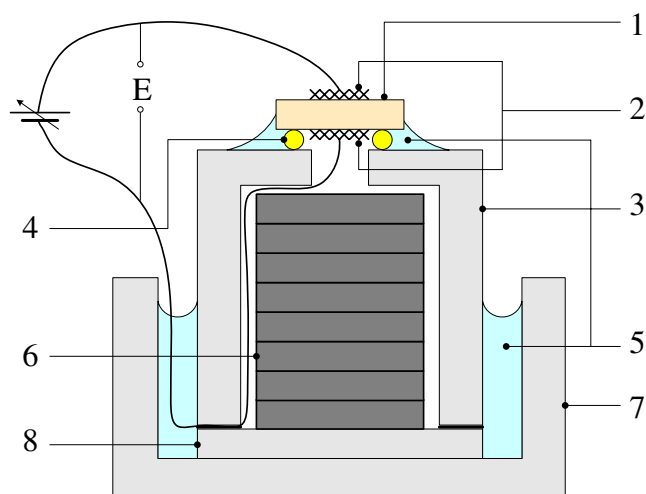

Fig. 15 The titration cell design suggested in [57]. *1*, YSZ electrolyte; *2*, Pt gauze; *3*, alumina cup; *4*, gold-ring gasket; *5*, borosilicate glass; *6*, specimen pellets; *7*, alumina crucible; *8*, alumina disk

studied with the use of a TGA system based on a Cahn D-200 microbalance with a sensitivity of 1 μg. For reduction of vibration effects, independent bearings for the −furnace and balance were used. The whole measuring system was fit with a vibration-suppressing unit and placed in a room where temperature and humidity were maintained to within ±0.1 °C and ±2%, respectively. This system allowed measurements with accuracy to 1–2 μg at temperatures from 800 to 1200 °C. The oxygen partial pressure within 10^{-18}–10^{-1} atm was monitored by the YSZ sensor located immediately near a sample. For coulometric titration at temperatures from 800 to 1000 °C, the system described in [57] was used (Fig. 15). As seen from Fig. 16, the results obtained by different methods are in good agreement. Although the certain advantage of thermogravimetry is a wider temperature range of measurements, coulometric titration provides greater resolution. In [58], which is a good example of exclusive accuracy of the method, isotherms with two inflection points were obtained in the titration of alumina-doped $SrTiO_{3-\delta}$. Assuming that these inflections reflect variations in the oxidation degree of impurity manganese cations, the authors described the experimental data and determined the concentration of impurities, which was as small as 80 ppm.

High standards of measurements were demonstrated in works [55, 56, 77, 83]. As seen in Fig. 17, the main features of the measuring arrangement included a double-wall alumina cell and a small-area electrochemical element, and they aimed at minimization of oxygen leaks similar to [57, 58, 64, 80, 81]. Measurements were carried out in
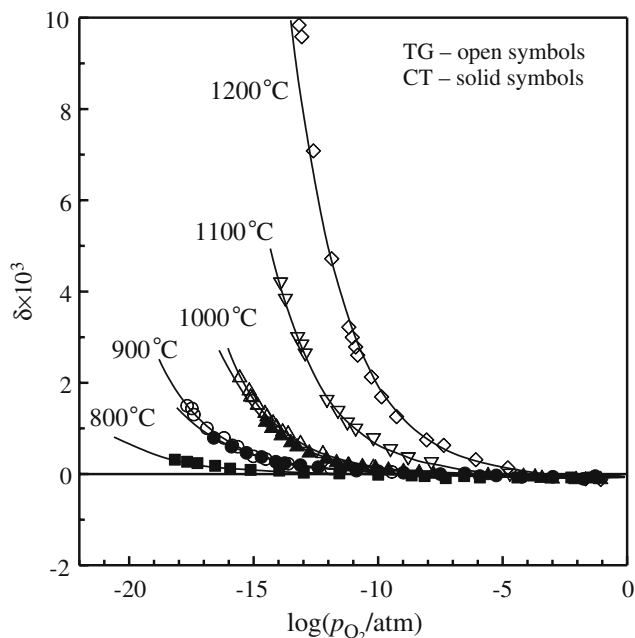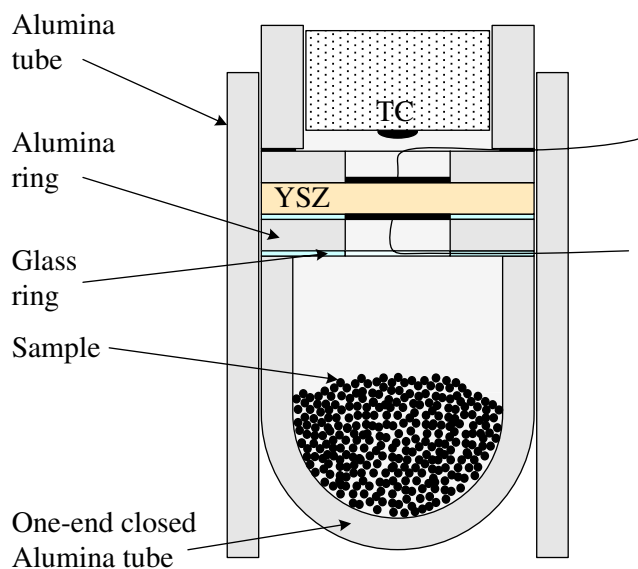

Fig. 17 A sketch of the coulometric titration cell suggested in [83]

isothermal mode at temperatures 750–1040 °C. The sensor potential variations less than 0.1%/minute were a criterion of equilibrium. For correction of possible errors related to oxygen leaks through microcracks, measurements at each temperature were performed in p_{O_2} increase and decrease modes. Electrochemical leaks for each experimental point were determined from Eq. 15 taking into account temperature, p_{O_2} gradient, and equilibration time. Upon respective corrections, the data were normalized to absolute values assuming that the stoichiometric state was achieved at minimum of the derivative $\partial\delta/p_{O_2}$ (Fig. 10a). Then, the isotherms obtained in pressure increase and decrease modes were averaged. The authors of [55, 56, 77, 83] studied perovskite-like iron-containing oxides where the oxygen homogeneous range is much wider than in titanites [57, 58, 80, 81]. This enabled obtaining of ample and precise data (Fig. 18).

An original modification of the method is proposed in [84, 85] and developed further by the authors of [86–88]. The experimental arrangement also enables the simultaneous measuring of oxygen chemical diffusion and surface exchange coefficients (Fig. 19). The cell includes a specimen pellet blocked electronically by the oxygen electrolyte slab at one surface. The opposite surface was made impermeable for oxygen ions by application of platinum foil. The cylindrical surface of the pellet was coated with gold and further sealed with glass [84, 89] to prevent direct oxygen ingress from ambient air. The gold layer prevented direct contact between the sample and the glass seal. An YSZ slab was used as the electrolyte. A thin layer of porous platinum was added between the pellet and the YSZ as a spacer to avoid undesired reaction between the components of the pellet and the zirconia [89]. The platinum

Fig. 16 The δ vs. $\log(p_{O_2}/\text{atm})$ plots for polycrystalline $TiO_{2-\delta}$ obtained from TG measurements and coulometric titration at different temperatures [81]
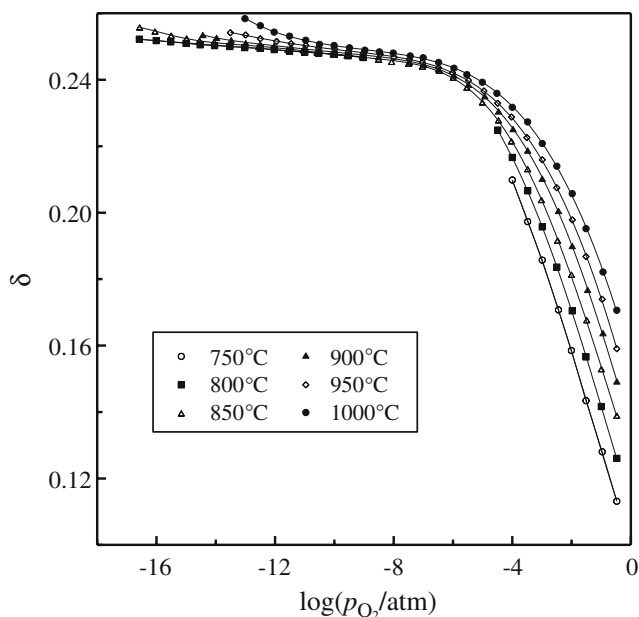
Fig. 18 The p_{O_2} dependences of non-stoichiometry in La$_{0.5}$Sr$_{0.5}$Ga$_{0.2}$Fe$_{0.8}$O$_{3-\delta}$ at different temperatures. *Lines* are guides to the eye [83]

was also presumed to act as a catalyst for the interfacial transport of oxygen. The opposite face of the electrolyte was coated with a thin layer of porous platinum in two separate patches to act as the air counter electrode and the reference electrode, as shown in Fig. 19. Figure 19b shows a variation of the design. Instead of having the electrolyte in direct contact with the specimen, a gold ring (50-mm thick) was added as a spacer. The upper surface of the electrolyte inside the gas spacer was again coated with a thin layer of porous Pt, such that the electrolyte acted as an oxygen pump. Because of the thermal expansion mismatch between the constituents of the cell, thermocycling had to be avoided in order to prevent cracking of the sample. Thus, the cells were heated up to the temperature of measurement (800–975 °C) only once. The cells, once cooled back to room temperature, were not used again. This implies that special care was required in the assembly of the cell to reach a satisfactory seal quality once the cell was heated [86]. Measurements with the use of such cells are carried out at constant temperature in the potential step mode, typically 20 mV [85]. Oxygen non-stoichiometry change at each step is determined from Eq. 19, while the chemical diffusion coefficient is determined by processing relaxation dependences on the basis of the second Fick law. Electrical impedance spectroscopy measurements with the use of the same cells allowed the determination of surface exchange coefficients of oxygen.

Oxygen non-stoichiometry was measured in the slow scan cycling voltammetry mode [87, 88], in which the response of the sample to a slow voltage sweep (3 μV/s)

was recorded. It was suggested that the chosen rate of potential change ensures the experimental conditions, at which a sample is close to equilibrium. The cell current was corrected for the contribution of leaks following [90]. The leak current was assumed to be a function of the reversible cell potential only, and in this way its contribution to the total cell current was suppressed by considering the difference between the oxidation and reduction currents $I = (I_{ox} - I_{red})/2$. The reversible potential difference (ΔE) across the oxygen pump, which is needed to evaluate the p_{O_2} in the gas space, can be estimated from the applied potential by correcting for the ohmic drop in the electrolyte and the polarization overpotential of the Pt electrodes in the presence of a current, both of which can be estimated from impedance measurements [87]. The change in oxygen non-stoichiometry for a given potential difference is then obtained by integrating the corrected cell current [87]:

$$\Delta\delta(\Delta E) = \frac{M_s}{m_s}\frac{1}{2F}\int_{E_0}^{E_0+\Delta E}\left[\frac{dE}{dt}\right]^{-1}I(\Delta E)dE \qquad (21)$$

where dE/dt is the scan rate. The corresponding non-stoichiometry data are shown in Fig. 20 along with the data obtained from potentiostatic measurements. Although the agreement between the two approaches is good at voltages larger than −100 mV, the difference reaches 10% at −150 mV. This indicates that the voltammetry deviates from the "close to equilibrium" condition at low p_{O_2}. This is probably due to the slowing of the reduction kinetics as the p_{O_2} decreases [88].

Oxygen adsorption of the surface of platinum was examined in [66]. The study required a high resolution, which can be achieved only by extremely careful minimization of all possible errors and, first of all, the error due to
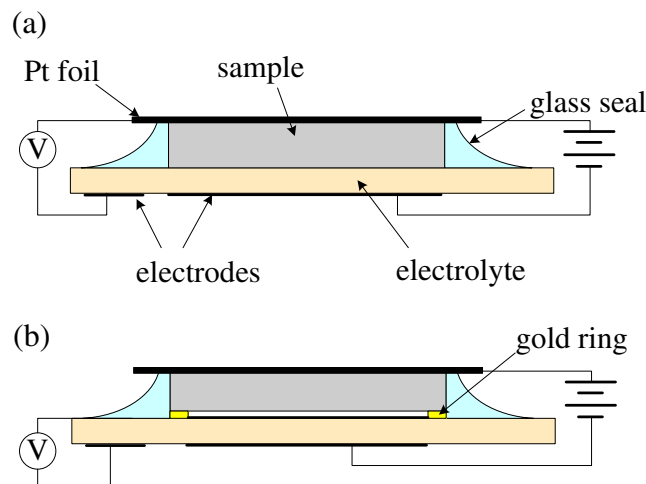

Fig. 19 Cell designs for potential step measurements: **a** blocked cell, **b** blocked cell with a gold ring spacer [86]
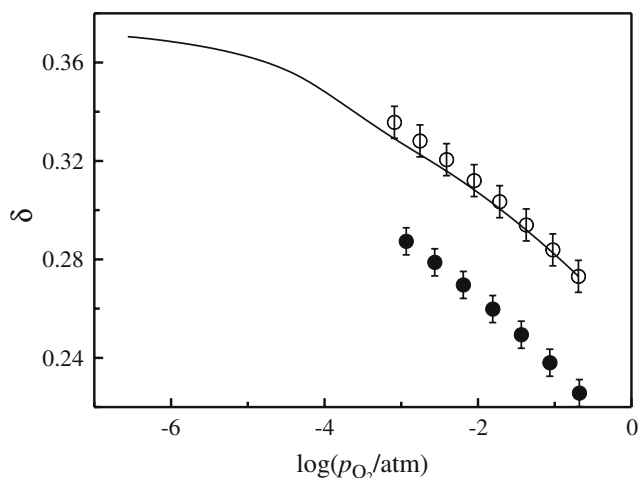
Fig. 20 Oxygen non-stoichiometry in $La_{0.4}Ba_{0.6}Fe_{0.8}Co_{0.2}O_{3-\delta}$ obtained from slow-scan cyclic voltammetry at 900 °C (*solid line*) and potential step measurements at 800 °C (*open circle*) and 900 °C (*filled circle*) [88]

electrochemical leaks. A specially designed cell with a compensation mode of operation was used (Fig. 21). In external and operating chambers of the cell, equal pressures were maintained with the aid of independent oxygen pumps. Although this cell certainly improves the quality of measurements, this design cannot be used extensively because running the system is not simple. Serious difficulties in sealing were noted even by the authors. The method was modified in [6] so that the external chamber is gasket-sealed in a cold zone (Fig. 22). The oxygen activity gradient between the external chamber and the internal cell was maintained within 1 mV during measurements, which decreased the leak rate by at least 100 times in a wide range of oxygen activity and ensured high measurement accuracy in the examination of small (0.1–0.3 g) oxide samples. The free volume of the measuring cell of ~0.3–0.5 ml was determined before the experiment with an accuracy ±0.01 ml by filling it with alcohol. The volume occupied by a sample was determined from the oxide density and mass. After the sample, whose mass was determined with an accuracy of ±0.0001 g, was placed in the measuring cell of the chamber, a high-temperature sealing paste was applied on the end face of the cell and a YSZ cover was attached. The assembly was placed into a tubular furnace, vacuumed, and filled with the gas mixture 90% O_2–10% CO_2, which enables relieving kinetic difficulties in the gas phase when measurements are performed under low oxygen activity. The assembly was heated to a temperature at which the sealing paste softens, and then it was cooled to operation temperature (950 °C). A cell is considered to be sealed if the change in the sensor reference potential (−20 mV) is not greater than 1 mV/h, which corresponds to the voltage drift due to electrochemical oxygen leaks through the cell walls when the pump of the isolating cell does not run. Coulometric

titration was performed in the isothermal mode. The oxygen pressure step was chosen to be $\Delta \log(p_{O_2}/atm) \sim 0.15$ and $\Delta \log(p_{O_2}/atm) \sim 0.3$ at $-4 < \log(p_{O_2}/atm) < 0.2$ and $-16 < \log(p_{O_2}/atm) < -4$, respectively. The data were registered after the equilibrium between the sample and the gas phase inside the measuring cell was attained. The change in the oxygen content in the sample was calculated from Eq. 7. The equilibrium criterion was taken as $d(\log(p_{O_2}/atm))/dt < 0.01$ hour^{-1}. Such experimental conditions usually ensure the reversibility of measurements at oxygen partial pressure cycling.

The main drawback of coulometric titration that hinders its application is the complexity of the preparatory work. Manufacturing of measuring cells requires much time and high accuracy of surface treatment. In some cases, before the beginning of important experiments, the cell is calibrated to determine the oxygen leak rate. Most often, the cell is used only in one experiment since its design does not ensure a non-destructive disassembly (e.g., Figs. 15 and 17). The authors of [74] attempted to construct a device for multiple coulometric measurements (Fig. 23). The device has a water-cooled sealing unit separating the tight alumina tube where a measured sample in an alumina crucible is placed. The measuring assembly with two electrochemical YSZ elements is located immediately above the sample. One element is used as an oxygen pump, the other as an activity sensor. To eliminate uncertainties in free volume determination, the authors used a strict dependence relating pressure and oxygen amount in the cell with geometric and temperature profiles along the cell. Oxygen leaks were
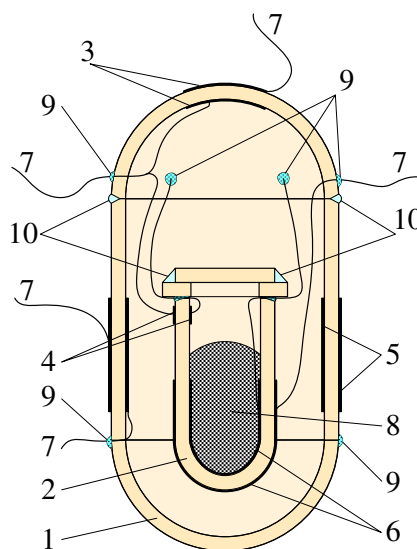

Fig. 21 The coulometric titration cell suggested in [66]. *1*, external chamber of solid electrolyte; *2*, operating chamber of solid electrolyte; *3* and *4*, oxygen sensors; *5* and *6*, oxygen pumps; *7*, current leads; *8*, specimen under study; *9*, high-temperature sealing cement; *10*, low-temperature sealing cement
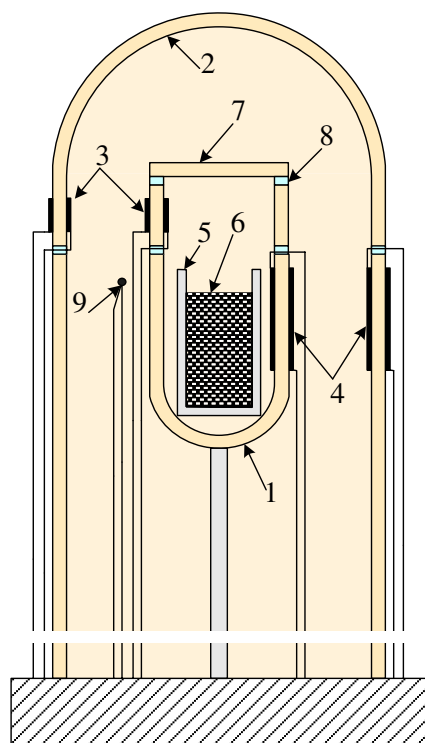
Fig. 22 The coulometric titration cell suggested in [6]. *1*, measuring cell of YSZ; *2*, isolating cell of YSZ; *3*, oxygen sensors; *4*, oxygen pumps; *5*, alumina crucible; *6*, sample; *7*, cover of YSZ; *8*, sealant; *9*, thermocouple

controlled oxygen partial pressure flows. The p_{O_2} before the sample is measured by the potentiometric zirconia sensor in CELL 1, while CELL 2, placed after the sample, is used as a pump/gauge system that sets a constant p_{O_2} by simultaneous oxygen electrochemical pumping and p_{O_2} measurement. In a steady state, the sample equilibrates with the surrounding atmosphere and the pumping current $I_{CELL\ 2}$ through CELL 2 is constant. When oxygen is released from the sample, the p_{O_2} in the carrier gas changes and $I_{CELL\ 2}$ decreases in order to maintain the previously adjusted p_{O_2} set point. After a new equilibrium between the sample and the carrier gas is attained, $I_{CELL\ 2}$ increases to the initial current level. The overall amount of oxygen released by the sample can be determined from the integral over the $I_{CELL\ 2}$ vs. time curve [94]. This method is advantageous to that employing the classical compact cell since it has no temperature limitations. At the same time, a rather complicated interpretation of measurement results may lead to greater errors. In addition, the necessity of using a gas carrier narrows the oxygen partial pressure range, in which measurements can be performed. In particular, oxygen non-stoichiometry in $La_{1-x}Sr_xCo_{1-y}Fe_yO_{3-\delta}$ was measured in [95] with the OXYLYT at temperatures 300–1000 °C and oxygen partial pressures $10^{-4.2}$–$10^{-2.9}$ atm. The oxygen non-stoichiometry in $La_{1-x}Sr_xCoO_{3-\delta}$ was examined in [96] with a similar device in the pressure range 10^{-4}–10^{-2} atm.

monitored in isothermal conditions by an approximation of experimental values with Eq. 18. As is seen from Fig. 24, this gives a rather rough description of the experimental data. The deviations are likely to be due to a considerable temperature gradient in the cell. In order to reduce the error, it makes sense to describe very precisely the experimental dependence of leak current on the oxygen activity gradient with the use of a polynomial or another function, which must not necessarily have a physical meaning. Another possibility for error reduction is to use the cell in the potentiostatic step titration mode, when leak current is accounted for at each step. In any case, the idea of creating a device for regular coulometric measurements should be supported and developed further.

Along with the application of small-sized measuring cells, sometimes the method is used where the cell with a sample is spatially separated from the system for electrochemical control of gas phase. There are works in which a commercial potentiometric–coulometric device OXYLYT (SensoTech Magdeburg, Germany) is used [91–93] (Fig. 25). The OXYLYT comprises two independent zirconia oxygen pump and gauge cells, designated as CELL 1 and CELL 2, respectively, and a temperature-programmed furnace in between the two cells, containing the sample. The two cells and the furnace are connected by stainless steel capillary tubes through which the carrier gas with
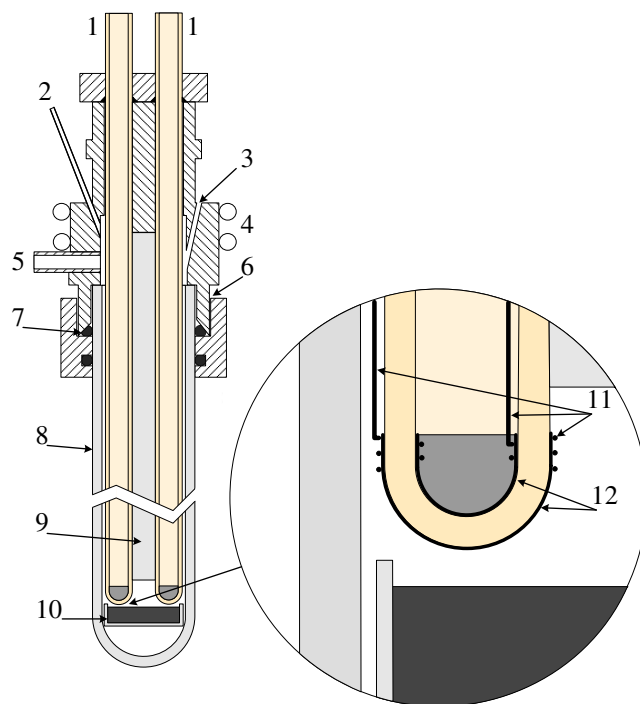

Fig. 23 The coulometric titration cell suggested in [74]. *1*, YSZ tube; *2*, gas inlet; *3*, hole for Pt wire (sealed); *4*, water cooling; *5*, gas outlet; *6*, brass coupling; *7*, O ring; *8*, alumina tube; *9*, alumina rod; *10*, alumina crucible with sample; *11*, Pt-wire; *12*, Pt electrodes
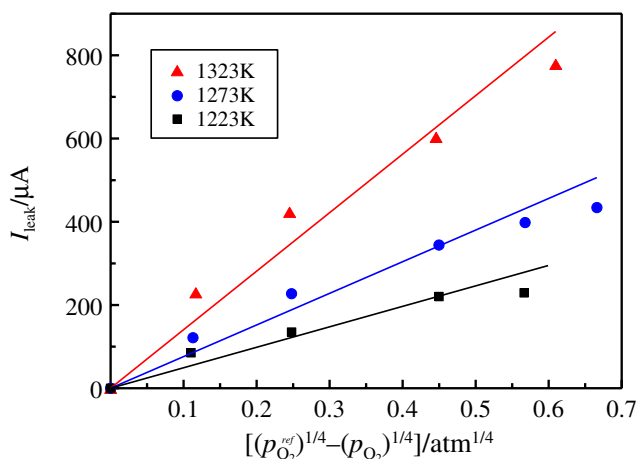
Fig. 24 Oxygen leak currents depending on pressure at different temperatures. The *straight lines* show best approximation of the data with Eq. 18 [74]

Simple applications of $p_{O_2} - T - \delta$ diagrams

Thermodynamic data characterizing the equilibrium with the gas phase are known for a great number of oxides. Probably, the most comprehensive studies of $p_{O_2} - T - \delta$ diagrams were performed for perovskite-like cuprates, in particular, the famous superconductor $YBa_2Cu_3O_{6+\delta}$, in which δ varies from 0 to 1 [21–24, 27, 97, 98]. There is ample information in the literature about the equilibrium oxygen content in cobaltites [3, 33, 73, 99, 100], ferrites [35, 45, 76, 77, 83, 101–103], and manganites [52, 74, 104, 105]. An analysis of the defect structure in oxides at elevated temperatures on the basis of $p_{O_2} - T - \delta$ diagrams makes it possible to obtain equilibrium constants of reactions and processes with participation of defects, as

well as chemical potentials and thermodynamic functions of oxygen in the oxide.

Partial thermodynamic functions of oxygen in $MO_{n-\delta}$ oxide can be calculated from oxygen chemical potential vs. temperature dependences at fixed δ values. The change in chemical potential $\Delta\mu_O$ of oxygen when it is transferred from the gas phase to the oxide is determined as

$$\Delta\mu_O(\delta, T) \equiv \mu_O^{MO_{n-\delta}} - \frac{1}{2}\mu_{O_2}^0 = RT \cdot \ln(p_{O_2}) \qquad (22)$$

where $\mu_{O_2}^0$ is the chemical potential of gaseous oxygen in standard state. Therefore, the equilibrium oxygen pressure values taken from the $p_{O_2} - T - \delta$ diagram permit the direct calculations of the $\Delta\mu_O(\delta, T)$ dependences. On the other hand, the change in the oxygen chemical potential is related to the change in the partial enthalpy and entropy of oxygen in the oxide as

$$\Delta\mu_O(\delta, T) = \Delta\overline{H}_O(\delta) - T\Delta\overline{S}_O(\delta) \qquad (23)$$

If $\Delta\overline{H}_O$ and $\Delta\overline{S}_O$ do not depend on temperature, which occurs most often, they are determined as

$$\Delta\overline{H}_O(\delta) = \left.\frac{\partial(\Delta\mu_O)}{\partial(1/T)}\right|_\delta \quad \text{and} \quad \Delta\overline{S}_O(\delta) = \left.\frac{\partial(\Delta\mu_O)}{\partial(T)}\right|_\delta, \qquad (24)$$

The concentration dependences $\Delta\overline{H}_O(\delta)$ and $\Delta\overline{S}_O(\delta)$ allow the calculation of the equilibrium oxygen content for arbitrary temperature and p_{O_2} values within the entire thermodynamic stability range of a non-stoichiometric oxide. Also, these thermodynamic functions contain information on defect equilibria and interactions. Their analysis and comparison of calculated and experimental δ is most often carried out on the basis of point defect models [52,
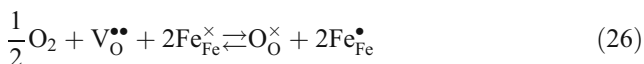
Fig. 25 Schematic representation (**a**) and measuring principle (**b**) of the solid electrolyte potentiometric–coulometric device OXYLYT [94]
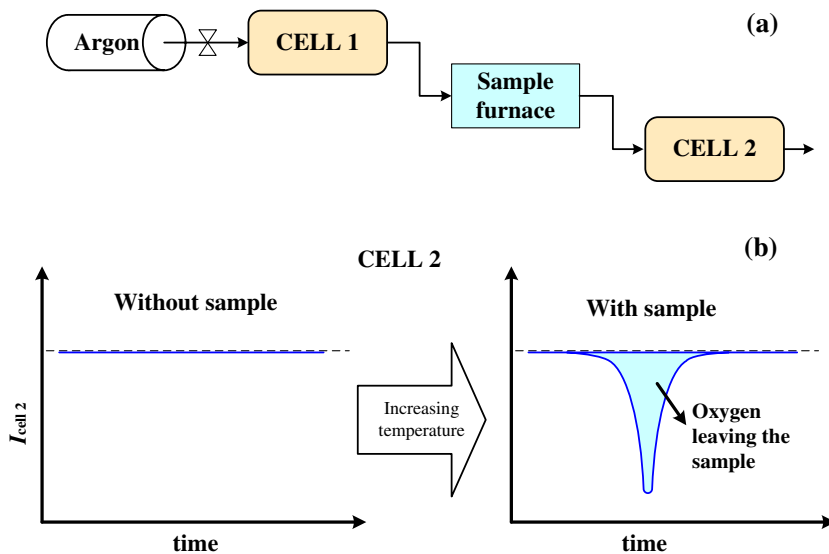
77, 83, 101, 104, 105]. It is instructive to briefly consider the defect structure studies [101] of solid solutions $La_{1-x}Sr_xFeO_{3-\delta}$ as an example. Figure 26 shows $\Delta\overline{H}_O(\delta)$ and $\Delta\overline{S}_O(\delta)$ dependences obtained from experimental results. It is seen that the oxidation of ferrites takes place in two stages. The smallest $\Delta\overline{H}_O(\delta)$ values correspond to the oxidation of $Fe^{2+}\left(Fe'_{Fe}\right)$ to $Fe^{3+}\left(Fe^{\times}_{Fe}\right)$.

$$\frac{1}{2}O_2 + V_O^{\bullet\bullet} + 2Fe'_{Fe} \rightleftarrows O_O^\times + 2Fe^\times_{Fe} \tag{25}$$
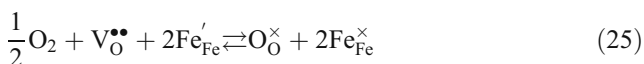
When the composition with $\delta = x/2$ is achieved, cations $Fe^{3+}\left(Fe^\times_{Fe}\right)$ begin to oxidize to $Fe^{4+}\left(Fe^\bullet_{Fe}\right)$

$$\frac{1}{2}O_2 + V_O^{\bullet\bullet} + 2Fe^\times_{Fe} \rightleftarrows O_O^\times + 2Fe^\bullet_{Fe} \tag{26}$$

Almost invariable $\Delta\overline{H}_O(\delta)$ values in the corresponding δ intervals are equal to enthalpies of oxidation reactions (25) and (26), ΔH^0_{Ox1} and ΔH^0_{Ox2}, respectively. Note that the difference $\left(\Delta H^0_{Ox2} - \Delta H^0_{Ox1}\right)$ equals the doubled enthalpy ΔH^0_{Disp} of the disproportionation reaction

$$2Fe^\times_{Fe} = Fe'_{Fe} + Fe^\bullet_{Fe} \tag{27}$$

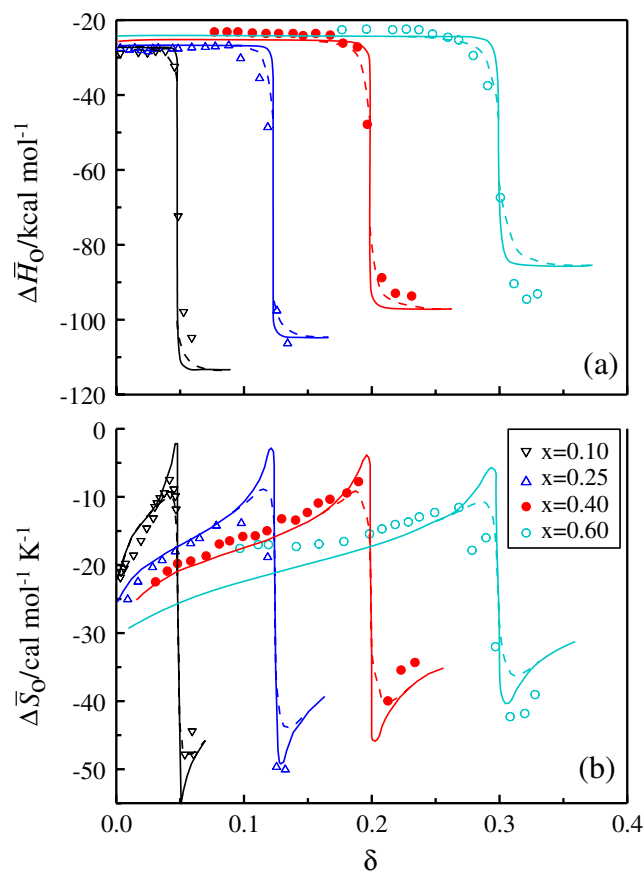**Fig. 26** The partial molar enthalpy (**a**) and entropy (**b**) of oxygen in $La_{1-x}Sr_xFeO_{3-\delta}$. *Points* are calculation results according to Eq. 24. *Lines* show the calculation results according to Eqs. 30 and 31 at 900 °C (*straight line*) and at 1200 °C (*dashed line*) [101]

Calculations [101] give the configuration entropy of oxygen in the ferrite as

$$s_O(conf) = R\left(\ln\frac{\delta\left[Fe^\times_{Fe}\right]^2}{(3-\delta)\left[Fe^\bullet_{Fe}\right]^2} + \frac{\partial\left[Fe'_{Fe}\right]}{\partial\delta}\ln K_{Disp}\right), \tag{28}$$

where

$$\frac{\partial\left[Fe'_{Fe}\right]}{\partial\delta} = 1 + \frac{2\delta - x}{4K_{Disp}\left[Fe^\times_{Fe}\right] + \left[Fe'_{Fe}\right] + \left[Fe^\bullet_{Fe}\right]} \tag{29}$$

and relations of partial molar functions with standard enthalpies $\left(\Delta H^0_{Ox2}, \Delta H^0_{Disp}\right)$ and entropies $\left(\Delta S^0_{Ox2}, \Delta S^0_{Disp}\right)$ for reactions (26) and (27)

$$\Delta\overline{H}_O(\delta) = \Delta H^0_{Ox2} - \frac{\partial\left[Fe'_{Fe}\right]}{\partial\delta}\Delta H^0_{Disp} \tag{30}$$

$$\Delta\overline{S}_O(\delta) = \Delta S^0_{Ox2} - \frac{\partial\left[Fe'_{Fe}\right]}{\partial\delta}\Delta S^0_{Disp} + s_O(conf) \tag{31}$$

The equilibrium constants for reactions (26) and (27) can be represented as

$$K_{Ox2} = \frac{\left[O_O^\times\right]\left[Fe^\bullet_{Fe}\right]^2}{p_{O_2}^{1/2}\left[V_O^{\bullet\bullet}\right]\left[Fe^\times_{Fe}\right]^2} \text{ and } K_{Disp} = \frac{\left[Fe'_{Fe}\right]\left[Fe^\bullet_{Fe}\right]}{\left[Fe^\times_{Fe}\right]^2}, \tag{32}$$

or

$$K_{Ox2} = \frac{(3-\delta)(x-2\delta)^2}{p_{O_2}^{1/2}(1-x+2\delta)^2} \text{ and } K_{Disp} = \frac{\delta p_{O_2}^{1/2}}{3-\delta}K_{Ox2} \tag{33}$$

in terms of measurable parameters δ and x. Further, Arrhenius plots for K_{Ox2} and K_{Disp} can be utilized in order to find $\left(\Delta H^0_{Ox2}, \Delta H^0_{Disp}\right)$ and $\left(\Delta S^0_{Ox2}, \Delta S^0_{Disp}\right)$. The use of these parameters in Eqs. 30 and 31 enables obtaining of oxygen partial enthalpy and entropy in $La_{1-x}Sr_xFeO_{3-\delta}$. A comparison of the calculated and measured $\Delta\overline{H}_O(\delta)$ and $\Delta\overline{S}_O(\delta)$ values shows a quite satisfactory coincidence, thus demonstrating a correct understanding of the defect structure in $La_{1-x}Sr_xFeO_{3-\delta}$ at least within experimentally studied limits of oxygen partial pressure, temperature, and strontium concentration [101].

The authors of [105] were among the first ones to observe that the $p_{O_2} - T - \delta$ diagram is a straightforward tool to reveal defect clustering. It was noticed that the appearance of even the simplest defect clusters $< M' - V_O^{\bullet\bullet} - M' >$

$$MO_n = M^\times_{n-2\delta} < M' - V_O^{\bullet\bullet} - M' >_\delta O_{n-\delta} + \frac{\delta}{2}O_2 \tag{34}$$
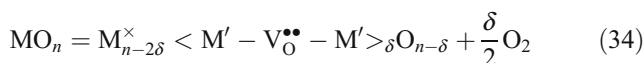
may result in oxygen deficiency proportional to $p_{O_2}^{-1/2}$ as it follows from the equilibrium constant

$$K = \frac{\delta p_{O_2}^{1/2}}{(n-\delta)(1-2\delta)^2}, \tag{35}$$

at a small concentration of oxygen vacancies, while the formation of isolated point defects, B' and $V_O^{\bullet\bullet}$, should better correspond to $\delta \sim p_{O_2}^{-1/6}$. It is clearly seen in Fig. 27 that the model of associated defects provides a rather accurate fitting of $p_{O_2} - \delta$ isotherms in LaMnO$_{3-\delta}$ [106] and LaCoO$_{3-\delta}$ [107], whereas the random defect model fails to give any satisfactory agreement with the experiment.

A deeper insight into the equilibrium diagrams, inter-ionic interactions, and the rough features of the electronic spectrum in the oxide can be obtained beyond the bounds of the equilibrium constant formalism. For instance, the authors of [4, 28] suggested the use of the equilibrium condition for oxygen exchange reaction

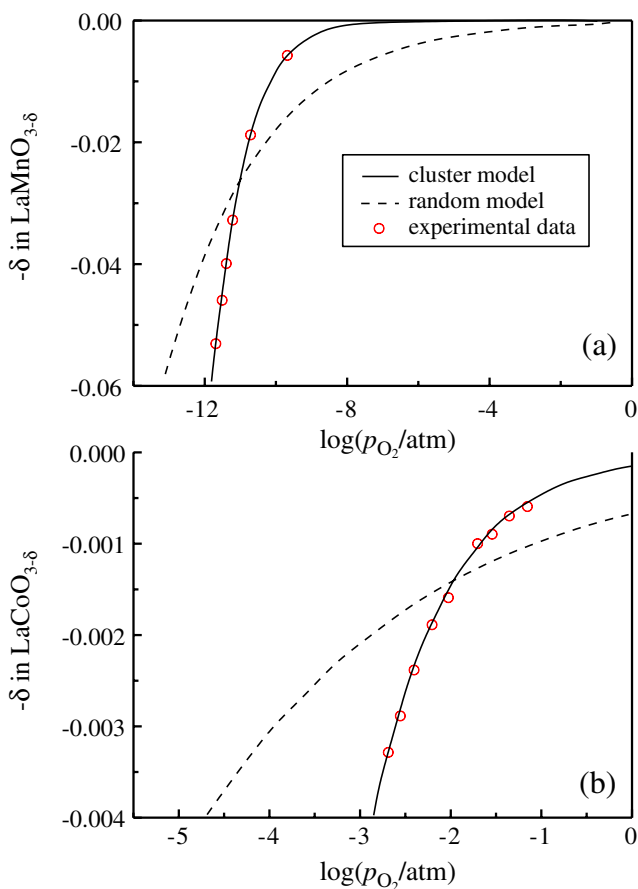$$\frac{1}{2}\mu_{O_2} = \mu_i + \alpha\mu_{h^+} \tag{36}$$

Fig. 27 The $p_{O_2} - \delta$ isotherms of LaMnO$_{3-\delta}$ (a) and LaCoO$_{3-\delta}$ (b) as calculated in the models of associated defects and random vacancies distribution [105]. Experimental points are taken from [106] (1200 °C) and [107] (963 °C), respectively
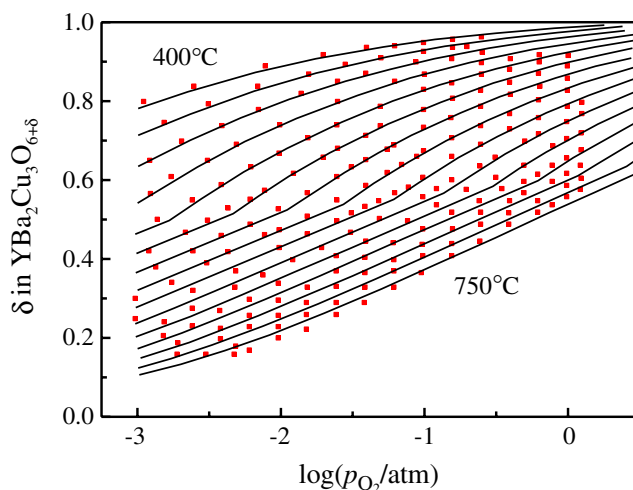

Fig. 28 $p_{O_2} - T - \delta$ diagram of YBa$_2$Cu$_3$O$_{3-\delta}$. Solid lines, 25 K step isotherms calculated by Eq. 37 [28]. Experimental points are taken from [27]

in the form

$$\ln p_{O_2} = \frac{1}{RT}$$
$$\times \left[-\mu_{O_2}^o(T) + 2\mu_i(T, \delta, \{P_i\}) + 2\mu_h(T, \delta, \{P_h\}) \right] \tag{37}$$

where $\{P_i\}$ and $\{P_h\}$ are model parameters for ionic and electronic subsystems. Chemical potentials μ_i and μ_h in the right-hand part of Eq. 37 can be calculated at different δ and T for assumed electronic structure and ion interaction models. The fitting of the calculated $\ln p_{O_2}$ values to experimental data enables one to calculate parameters $\{P_i\}$ and $\{P_h\}$ that describe ion and electron subsystems. This procedure was applied to YBa$_2$Cu$_3$O$_{6+\delta}$. It is shown that a fairly satisfactory approximation of the experimental $p_{O_2} - T - \delta$ diagram (Fig. 28) can be achieved when a simple model of the Bethe–Kikuchi type is used for the description of oxygen ion interactions while the electronic structure is approximated by a two-dimensional parabolic valence band with delocalized states above it.

Conclusion

Oxygen non-stoichiometry is one of the most important characteristics of oxide materials. The oxygen changes in composition with temperature, oxygen activity in the ambient atmosphere, concentration of impurities and dopants reflect the formation of ionic and electronic defects and their interaction in oxides. The respective $p_{O_2} - T - \delta$ diagrams can be obtained by a variety of techniques. The coulometric titration is distinguished by high precision,

which is difficult to achieve with the use of other methods, and it is particularly advantageous for the application at small activities of oxygen, $p_{O_2} < 10^{-5}$ atm. Additional merit includes the availability of experimental apparatus. However, an implementation of the method requires substantial manual work, particularly thorough the preparation of experimental cells and careful accounting of the errors that may enter the experimental data. The serious drawback of coulometric titration is the limited, often one-time, use of the titration cells though attempts are known of inventions nearing commercial standards for scientific equipment. Another issue is due to the small oxygen conductivity of modern zirconia-based electrolytes that hampers the measurements at temperatures below 650 °C. Though different approaches are known to overcome this limitation, it is quite possible that the development of novel electrolytes with better-conducting properties will add substantially to the method.

References

1. Kröger FA (1964) The chemistry of imperfect crystals. North-Holland, Amsterdam
2. Karen P (2006) J Solid State Chem 179:3167–3183
3. Lankhorst MHR, Bouwmeester HJM, Verweij H (1997) J Solid State Chem 133:555–567
4. Tsidilkovskii VI, Leonidov IA, Lakhtin AA, Mezrin VA (1991) Phys Status Solidi B 163:231–240
5. Kanai H, Hashimoto T, Tagawa H, Mizusaki J (1997) Solid State Ion 99:193–199
6. Mitberg EB, Patrakeev MV, Lakhtin AA, Leonidov IA, Kozhevnikov VL, Poeppelmeier KR (1999) Solid State Ion 120:239–249
7. Kuhn JN, Matter PH, Millet JMM, Watson RB, Ozkan US (2008) J Phys Chem C 112:12468–12476
8. Katsuki M, Wang S, Yasumoto K, Dokiya M (2002) Solid State Ion 154–155:589–595
9. Katsuki M, Wang S, Dokiya M, Hashimoto T (2003) Solid State Ion 156:453–461
10. Bucher E, Sitte W, Caraman GB, Cherepanov VA, Aksenova TV, Ananyev MV (2006) Solid State Ion 177:3109–3115
11. Otake T, Yugami H, Yashiro K, Nigara Y, Kawada T, Mizusaki J (2003) Solid State Ion 161:181–186
12. Oishi M, Yashiro K, Sato K, Mizusaki J, Kawada T (2008) J Solid State Chem 181:3177–3184
13. Mizusaki J, Hasegawa M, Yashiro K, Matsumoto H, Kawada T (2006) Solid State Ion 177:1925–1928
14. Oishi M, Yashiro K, Hong JO, Nigara Y, Kawada T, Mizusaki J (2007) Solid State Ion 178:307–312
15. Hashimoto T, Kobayashi T, Tanaka H, Hirasawa R, Hirai H, Tagawa H (1998) Solid State Ion 108:371–376
16. Wang S, Inaba H, Tagawa H, Dokiya M, Hashimoto T (1998) Solid State Ion 107:73–79
17. Kobayashi T, Wang S, Dokiya M, Tagawa H, Hashimoto T (1999) Solid State Ion 126:349–357
18. Yang Z, Lin YS (2002) Solid State Ion 150:245–254
19. Kim S, Merkle R, Maier J (2004) Surf Sci 549:196–202
20. Onuma S, Yashiro K, Miyoshi S, Kaimai A, Matsumoto H, Nigara Y, Kawada T, Mizusaki J, Kawamura K, Sakai N, Yokokawa H (2004) Solid State Ion 174:287–293
21. Kishio K, Shimoyama J, Hasegawa T, Kitazawa K, Fueki K (1987) Jpn J Appl Phys 26:L1228–L1230
22. Specht ED, Sparks CJ, Dhere AG, Brynestad J, Cavin OB, Kroeger DM, Oye HE (1988) Phys Rev B 37:7426–7434
23. Yamaguchi S, Terabe K, Saito A, Yanagi S, Iguchi Y (1988) Jpn J Appl Phys 27:L179–L181
24. Lindemer TB, Hunley JF, Gates JE, Sutton AL, Brynestad J, Hubbard R, Gallagher PK (1988) J Am Ceram Soc 72:1775–1786
25. Fueki K, Idemoto Y, Ishizuka H (1990) Phys C 166:261–265
26. Verweij H, Feiner LF (1990) Phys Rev B 41:4302–4308
27. Meuffels P, Naeven R, Wenzl H (1989) Phys C 161:539–548
28. Tsidilkovskii VI, Leonidov IA, Lakhtin AA, Mezrin VA (1991) Phys Status Solidi B 168:233–244
29. Schmidt M, Campbell SJ (2001) J Solid State Chem 156:292–304
30. McIntosh S, Vente JF, Haije WG, Blank DHA, Bouwmeester HJM (2006) Solid State Ion 177:833–842
31. Liu LM, Lee TH, Qiu L, Yang YL, Jacobson AJ (1996) Mater Res Bull 31:29–35
32. Grunbaum N, Mogni L, Prado F, Caneiro A (2004) J Solid State Chem 177:2350–2357
33. Søgaard M, Hendriksen PV, Mogensen M, Poulsen FW, Skou E (2006) Solid State Ion 177:3285–3296
34. Takeda Y, Kanno K, Takada T, Yamamoto Takano OM, Nakayama N, Bando Y (1986) J Solid State Chem 63:237–249
35. Patrakeev MV, Leonidov IA, Kozhevnikov VL, Kharton VV (2004) Solid State Sci 6:907–913
36. McIntosh S, Vente JF, Haije WG, Blank DHA, Bouwmeester HJM (2006) Chem Mater 18:2187–2193
37. Harvey AS, Litterst FJ, Yang Z, Rupp JLM, Infortuna A, Gauckler LJ (2009) Phys Chem Chem Phys 11:3090–3098
38. Bucher E, Egger A, Ried P, Sitte W, Holtappels P (2008) Solid State Ion 179:1032–1035
39. Nakayama N, Takano M, Inamura S, Nakanishi N, Kosuge K (1987) J Solid State Chem 71:403–417
40. Liu D, Yao X, Smyth DM, Bhalla AS, Cross LE (1993) J Appl Phys 74:3345–3356
41. Mitchell BJ, Rogan RC, Richardson JW, Ma B, Balachandran U (2002) Solid State Ion 146:313–321
42. Prado F, Mogni L, Cuello GJ, Caneiro A (2007) Solid State Ion 178:77–82
43. Dann SE, Weller MT, Currie DB (1992) J Solid State Chem 97:179–185
44. Shilova YA, Patrakeev MV, Mitberg EB, Leonidov IA, Kozhevnikov VL (2002) J Solid State Chem 168:275–283
45. Mogni L, Fouletier J, Prado F, Caneiro A (2005) J Solid State Chem 178:2715–2723
46. Prado F, Armstrong T, Caneiro A, Manthiram A (2001) J Electrochem Soc 148:J7–J14
47. Leonidov IA, Patrakeev MV, Kozhevnikov VL (2006) Russ J Phys Chem A 80:523–528
48. Mogni LV, Prado FD, Cuello GJ, Caneiro A (2009) Chem Mater 21:2614–2623
49. Tikhonovich VN, Zharkovskaya OM, Naumovich EN, Bashmakov IA, Kharton VV, Vecher AA (2003) Solid State Ion 160:259–270
50. Mizusaki J, Tagawa H, Naraya K, Sasamoto T (1991) Solid State Ion 49:111–118
51. Kanai H, Mizusaki J, Tagawa H, Hoshiyama S, Hirano K, Fujita K, Tezuka M, Hashimoto T (1997) J Solid State Chem 131:150–159

52. Mizusaki J, Mori N, Takai H, Yonemura Y, Minamiue H, Tagawa H, Dokiya M, Inaba H, Naraya K, Sasamoto T, Hashimoto T (2000) Solid State Ion 129:163–177

53. Nakamura T, Yashiro K, Sato K, Mizusaki J (2009) Solid State Ion 180:368–376

54. Schneider D, Gödickemeier M, Gauckler LJ (1997) J Electroceram 1:165–172

55. Yoo J, Jacobson AJ in Solid-State Ionic Devices III, Wachsman ED, Swider-Lyons K, Carolan MF, Garzon FH, Liu M, Stetter JR, Editors, PV 2002-26:354–363. The Electrochemical Society Proceedings Series, Pennington, NJ (2003)

56. Park CY, Azzarello FV, Jacobson AJ (2006) J Mater Chem 16:3624–3628

57. Lee D-K, Yoo H-I (2001) Solid State Ion 144:87–97

58. Shin C-J, Yoo H-I, Lee C-E (2007) Solid State Ion 178:1081–1087

59. Park J-H, Blumental RN (1989) J Electrochem Soc 136:2867–2876

60. Schmalzried H (1981) Solid state reactions. Chemie, Weinheim

61. Giddings RA, Gordon RS (1974) J Electrochem Soc 121:793–800

62. Patrakeev MV, Leonidov IA, Kozhevnikov VL (1995) Solid State Ion 82:5–13

63. Dalslet BT, Søgaard M, Bouwmeester HJM, Hendriksen PV (2009) Solid State Ion 180:1173–1182

64. Kang S-H, Yoo H-I (1996) Solid State Ion 86–88:751–755

65. Tretyakov YUD, Komarov VF, Prosvirina NA, Kutsenok IB (1972) J Solid State Chem 5:157–167

66. Kuzin BL, Komarov MA (1990) Solid State Ion 39:163–172

67. Tikhonovich VN, Naumovich EN, Logvinovich DI, Kharton VV, Vecher AA (2003) J Solid State Electrochem 7:77–82

68. Chatzichristodoulou C, Hendriksen PV (2010) J Electrochem Soc 157:B481–B489

69. Gellings PJ, Bouwmeester HJM (1997) The CRC handbook of solid state electrochemistry. CRC, Boca Raton

70. Lankhorst MHR, Bouwmeester HJM (1997) J Electrochem Soc 144:1261–1267

71. Lankhorst MHR, Bouwmeester HJM, Verweij H (1997) Solid State Ion 96:21–27

72. Lankhorst MHR, Bouwmeester HJM (1997) J Electrochem Soc 144:1268–1273

73. Mizusaki J, Mima Y, Yamauchi S, Fueki K, Tagawa H (1989) J Solid State Chem 80:102–111

74. Bakken E, Norby T, Stølen S (2005) Solid State Ion 176:217–223

75. Wagner C (1971) Prog Solid State Chem 6:1–15

76. Mizusaki J, Yoshihiro M, Yamauchi S, Fueki K (1985) J Solid State Chem 58:257–266

77. Park CY, Jacobson AJ (2005) J Electrochem Soc 152:J65–J73

78. Patrakeev MV, Kharton VV, Bakhteeva YuA, Shaula AL, Leonidov IA, Kozhevnikov VL, Naumovich EN, Yaremchenko AA, Marques FMB (2006) Solid State Sci 8:476–487

79. Tikhonovich VN, Naumovich EN, Kharton VV, Yaremchenko AA, Kovalevsky AV, Vecher AA (2002) Electrochimica Acta 47:3957–3964

80. Lee D-K, Yoo H-I, Becker KD (2002) Solid State Ion 154–155:189–193

81. Lee D-K, Jeon J-I, Kim M-H, Choi W, Yoo H-I (2005) J Solid State Chem 178:185–193

82. Xue J, Dieckmann R (1991) J Electrochem Soc 138:36C–40C

83. Yoo J, Jacobson AJ (2009) J Electrochem Soc 156:B1085–B1091

84. Belzner A, Gür TM, Huggins RA (1990) Solid State Ion 40–41:535–538

85. Belzner A, Gür TM, Huggins RA (1992) Solid State Ion 57:327–337

86. Diethelm S, Closset A, Nisancioglu K, Van Herle J, McEvoy AJ, Gür TM (1999) J Electrochem Soc 146:2606–2612

87. Diethelm S, Closset A, Van herle J, Nisancioglu K (2000) Electrochemistry 68:444–450

88. Diethelm S, Van Herle J (2004) Solid State Ion 174:127–134

89. Sunde S, Nisancioglu K, Gür TM (1996) J Electrochem Soc 143:3497–3504

90. Jacobsen T, Zachau-Christiansen B, West K, Skaarup S (1991) Proc. 2nd Int. Symp. SOFC, Athens, Commission of the European Communities, Luxembourg, 795

91. Trofimenko NE, Ullmann H, Paulsen J, Müller R (1997) Solid State Ion 201-214

92. Vashuk VV, Kokhanovskii, Yuskevich (2000) Inorganic Materials 36:79-83

93. Vashook V, Girdauskaite E, Zosel J, Wen T-L, Ullmann H, Guth U (2006) Solid State Ion 177:1163–1171

94. Figueiredo FM, Waerenborgh J, Kharton VV, Näfe H, Frade JR (2003) Solid State Ion 156:371–381

95. Mantzavinos D, Hartley A, Metcalfe IS, Sahibzada M (2000) Solid State Ion 134:103–109

96. Sitte W, Bucher E, Preis W (2002) Solid State Ion 154–155:517–522

97. Strobel P, Capponi JJ, Marezio M, Monod P (1987) Solid State Comm 64:513–515

98. Patrakeev MV, Mitberg EB, Lakhtin AA, Leonidov IA, Kozhevnikov VL, Poeppelmeier KR (1998) Ionics 4:191–199

99. Petrov AN, Cherepanov VA, Kononchuk OF, Gavrilova LY (1990) J Solid State Chem 87:69–76

100. Frontera C, Caneiro A, Carillo AE, Oró-Solé J, García-Munoz JL (2005) Chem Mater 17:5439–5445

101. Mizusaki J, Yoshishiro M, Yamauchi S, Fueki K (1987) J Solid State Chem 67:1–8

102. Holt A, Norby T, Glenne R (1999) Ionics 5:434–443

103. Markov AA, Savinskaya OA, Patrakeev MV, Nemudry AP, Leonidov IA, Pavlyukhin YT, Ishchenko AV, Kozhevnikov VL (2009) J Solid State Chem 182:799–806

104. Kuo JH, Anderson HU, Sparlin DM (1989) J Solid State Chem 83:52–60

105. Van Roosmalen JAM, Corfunke EHP (1994) J Solid State Chem 110:109–112

106. Seppanen M, Kyto M, Taskinen P (1980) Scand J Metal 9:3

107. Kamata K, Nakajama T, Hayashi T, Nakamura T (1978) Mater Res Bull 13:49–54